Endogenous bystander killing mechanisms enhance the activity of novel FAP-specific CAR-T cells against glioblastoma

Wenbo Yu[1, 2], Nga TH Truong[1, 2], Ruhi Polara[1], Tessa Gargett[1, 2, 3], Melinda N Tea[1], Stuart M Pitson[1,3], Michaelia P Cockshell[1], Claudine S Bonder[1, 3], Lisa M Ebert *[1, 2, 3] and Michael P Brown *[1, 2, 3]

[1] Centre for Cancer Biology, SA Pathology and University of South Australia, Australia
[2] Cancer Clinical Trials Unit, Royal Adelaide Hospital, Adelaide, SA, Australia
[3] Adelaide Medical School, The University of Adelaide, Adelaide, SA, Australia

* Co-senior authors.

Running Title: Bystander killing enhances FAP-CAR-T cells targeting glioblastoma

Corresponding Author:
Lisa M Ebert
Centre for Cancer Biology, UniSA Bradley Building
North Terrace, Adelaide, SA 5000, Australia
email lisa.ebert@sa.gov.au
Phone: +61 8 8302 7817

Abstract

Objectives: CAR-T cells are being investigated as a novel immunotherapy for glioblastoma, but clinical success has been limited. We recently described fibroblast activation protein (FAP) as an ideal target antigen for glioblastoma immunotherapy, with expression on both tumor cells and tumor blood vessels. However, CAR-T cells targeting FAP have never been investigated as a therapy for glioblastoma.

Methods: We generated a novel FAP targeting CAR with CD3ζ and CD28 signaling domains and tested the resulting CAR-T cells for their lytic activity and cytokine secretion function *in vitro* (using real-time impedance, flow cytometry, imaging, and bead-based cytokine assays), and *in vivo* (using a xenograft mimicking the natural heterogeneity of human glioblastoma).

Results: FAP-CAR-T cells exhibited target specificity against model cell lines and potent cytotoxicity against patient-derived glioma neural stem cells, even when only a subpopulation expressed FAP, indicating a bystander killing mechanism. Using co-culture assays, we confirmed FAP-CAR-T cells mediate bystander killing of antigen-negative tumor cells, but only after activation by FAP-positive target cells. This bystander killing was at least partially mediated by soluble factors and amplified by IL-2 which activated the non-transduced fraction of the CAR-T product. Finally, a low dose of intravenously administered FAP-CAR-T cells controlled, without overt toxicity, the growth of subcutaneous tumors created using a mixture of antigen-negative and antigen-positive glioblastoma cells.

Conclusions: Our findings advance FAP as a leading candidate for clinical CAR-T therapy of glioblastoma and highlight under-recognized antigen non-specific mechanisms that may contribute meaningfully to the antitumor activity of CAR-T cells.

Key words: CAR-T, glioblastoma, cancer immunotherapy, bystander killing, bystander activation, fibroblast activation protein, glioma neural stem cells.

INTRODUCTION

Glioblastoma is the most lethal form of primary brain tumor and there is an urgent need for more effective therapies. Despite receiving intensive treatment upon initial diagnosis with all three classical pillars of cancer therapy (surgery, radiotherapy, and chemotherapy), patients almost inevitably relapse within a matter of months[1]. There is no standard treatment for recurrent glioblastoma, and most patients will die within 6 months of recurrence [2]. The recent emergence of a 'fourth pillar' of cancer treatment, immunotherapy, may provide new hope that this dismal picture can be changed for patients with glioblastoma soon.

Chimeric antigen receptor (CAR)-T cells are one of the success stories of cancer immunotherapy, but so far clinical impacts are limited to B-cell malignancies. There remain significant hurdles to overcome before this success can be extended to solid tumors [3]. One clear challenge is the lack of ideal target antigens in solid tumors. This sits in contrast to B-cell malignancies where lineage markers, such as CD19, show near-ubiquitous expression on cancerous cells and no expression outside the hematologic compartment. Nevertheless, the possibility of adapting CAR-T cell therapy to the treatment of glioblastoma is under extensive investigation [4]. Most interest to date for clinical CAR-T targeting of glioblastoma has focused

68 on targeting the antigens EGFRvIII, HER2 and IL-13R2α [5-12]. Positive outcomes from clinical
69 trials to date have generally been modest. However, some tumor regressions have been
70 observed in recent studies, particularly using localized delivery of CAR-T cells, although such
71 responses are generally transient [7, 11, 12]. Given the profound tumor heterogeneity of
72 glioblastoma, identification of more and better targets is a key focus of research. This should
73 be coupled with the identification of innovative approaches to broaden CAR-T cell reactivity.

74 Fibroblast activation protein (FAP) is a surface-expressed proteolytic enzyme that is well
75 known for its expression in cancer-associated fibroblasts [13]. Because of this, FAP has been
76 identified as a promising immunotherapy target for carcinomas which are typically heavily
77 infiltrated with fibroblasts, such as those of prostate, breast, lung, and pancreas. In those
78 studies, FAP has primarily been investigated as the target of tumor supporting stroma [14-18],
79 but can also serve as a direct tumor target in certain cancers such as mesothelioma [19, 20]. We
80 and others found FAP to be consistently over-expressed in glioblastoma compared to normal
81 brain, although we failed to find fibroblast expression of FAP in glioblastoma [21, 22]. Rather, our
82 detailed expression analyses of all cell types in glioblastoma revealed heterogeneous
83 expression of FAP on the tumor cells, coupled with near-ubiquitous expression around tumor
84 blood vessels, with expression observed on both endothelial cells and pericytes. These studies
85 suggest FAP is an ideal immunotherapy target for glioblastoma, as it should allow targeting of
86 not only tumor cells, but also the tumor's supporting vascular networks [21].

87 Several FAP-specific CARs have been described in the literature. All FAP-CARs have been
88 derived from one of four mouse monoclonal antibodies (mAbs). A CAR developed from the
89 FAP-5 mAb cross-reacts with both mouse and human FAP. However, FAP-5-CAR-T cells

90 showed serious toxicities in mice and this CAR has not been pursued further [23]. A second CAR
91 developed from the F19 mAb recognizes only human FAP, thus this CAR could not be used to
92 test potential host FAP-related toxicities in mouse models [19, 20, 24]. A third CAR developed from
93 mAb 73.3 cross-reacts with both mouse and human FAP and showed limited toxicities in mice
94 [16, 17]. CAR-T cells derived from both F19 and 73.3 mAbs showed antitumor effects in mouse
95 models of multiple types of transplanted tumors [16, 20] and have now progressed into phase 1
96 clinical trials (ClinicalTrials.gov Identifiers: NCT039325652019 and NCT017221492015).
97 However, neither CAR-T has been tested on glioblastoma. F19-CAR-T cells were well tolerated
98 clinically [25], although no detailed report of either trial has been released yet.

99 In this study, we generated a FAP-specific CAR derived from the MO36 mAb, which was
100 selected from phage display and recognizes both murine and human FAP [26]. Another CAR
101 based on MO36 previously showed antitumor effects in a lung cancer mouse model without
102 toxicity [15]. We tested FAP-CAR-T cell function using model cell lines, tumor cells expanded
103 from patient glioblastoma tissues, and a mouse model designed to recapitulate the natural
104 heterogeneity of glioblastoma. In addition to confirming the specificity and activity of FAP-
105 CAR-T cells, we also uncovered a potent bystander killing mechanism that could facilitate
106 more complete tumor destruction than would be predicted by antigen expression alone.

107

108 **RESULTS**

109 **Generation and production of CAR T cells targeting FAP**

110 Based on previous studies [15, 26], we designed and constructed a FAP-CAR comprising the MO36
111 single chain fragment-variable (scFv), a myc epitope tag, a long spacer, and CD28 and CD3ζ
112 signaling domains (Figure. 1a). This CAR transgene was integrated in CD3/CD28-activated
113 human T cells via lentiviral transduction. CAR expression on transduced T cells was assessed
114 by flow cytometry (Figure. 1b). Transduction efficiency values sufficient to test CAR-T cell
115 function (mean 25.1%, SD 7.2% from transduction of 8 donors) were achieved using
116 unconcentrated viral supernatant.

117 CAR-T cell responses to FAP stimulation *in vitro* were initially measured by co-culturing CAR-T
118 cells with FAP-expressing long-term cancer cell lines. The RPMI-7951 melanoma cell line,
119 which expresses uniformly high levels of FAP, was used for initial testing of FAP-CAR-T cells,
120 while the FAP-negative U251 glioblastoma cell line was used as a negative control (Figure 1c).
121 These tumor cell lines were co-cultured with FAP-CAR-T cells or CAR-T cells targeting an
122 irrelevant antigen (EphA3) for 48 hours, and the level of IL-2 in the culture supernatant was
123 measured by ELISA (Figure 1d). The data indicate that FAP-CAR-T cells (but not irrelevant CAR-
124 T cells) responded specifically to target cells expressing FAP, whereas there was no response
125 to cells lacking FAP. Further analysis of the CAR-T cells from 5 donors revealed a relatively
126 balanced CD4:CD8 ratio and dominant populations of effector memory (TEM) and terminally
127 differentiated effector (TEMRA) cells within the cell products (Figure 1 e-f).

128

129 **Cytotoxicity of FAP-CAR-T cells against glioblastoma cell lines and patient-derived glioma**
130 **neural stem (GNS) cells**

131 We next used impedance-based real-time analysis to assess FAP-CAR-T cell cytotoxicity. As
132 target cells, the FAP-expressing U87 human glioblastoma cell line was compared with the FAP-
133 negative glioblastoma cell line U251 (Figure 2a). As expected, FAP-CAR-T cells were strongly
134 cytotoxic against U87 target cells, whereas non-transduced T cells (NT-T) induced only
135 minimal background lysis. FAP-CAR-T cells failed to lyse U251 cells above background levels,
136 thereby confirming the specificity of the CAR.

137 Although long-term established cell lines such as U87 provide a suitable model to test a
138 diverse range of therapeutic approaches, these cells may not adequately represent primary
139 glioblastoma cells. Therefore, we next selected a panel of patient-derived glioma neural stem
140 (GNS) cells as a more biologically relevant type of target cell to test the cytotoxic activity of
141 our FAP-CAR-T cells. We checked a panel of different GNS cells for FAP expression and chose
142 three cultures which express different levels of FAP. CCB-G3-C, MN1, and CCB-G6-T are
143 representative of high, medium, and low level FAP expression, respectively (Figure 2b). We
144 found substantial killing of all of three GNS cell lines (Figure 2b). Of note, when cultured with
145 MN1 cells, which are <50% FAP^+, the FAP-CAR-T cells induced near-complete cytotoxicity (> 90%
146 lysis). Even more remarkably, in the case of CCB-G6-T cells, even a 10% FAP^+ population was
147 sufficient to induce the lysis of >80% of all target cells.

148 These observations suggest that FAP-CAR-T cells are capable of potent bystander killing,
149 whereby activation of CAR-T cells by a subpopulation of antigen-expressing target cells leads
150 to killing of antigen-negative tumor cells as well [27]. This idea was further supported by a

151 simple flow cytometry assay, wherein CCB-G6-T target cells were co-cultured with FAP-CAR-T
152 cells for 48 hours and the residual viable cells assessed for FAP expression (Supplementary
153 Figure 1). After this time, the small FAP^+ population within CCB-G6-T was significantly
154 depleted, as expected. Notably, however, the loss in cell viability amongst the entire target
155 cell population was ~50%, far more than the FAP^+ population frequency, further supporting a
156 bystander killing effect of FAP-CAR-T cells. The observed loss of FAP expression was unlikely to
157 be due to trogocytosis (27), as we did not detect any transfer of FAP to CAR-T cells (data not
158 shown). However, this assay did not allow definitive tracking of the fate of FAP^+ versus FAP^-
159 target cells, and so we sought a better system to address this issue more comprehensively.

160

161 **Confirmation that FAP-CAR-T cells induce antigen-dependent bystander killing of tumor cells**

162 To confirm the bystander killing capability of FAP-CAR-T cells, we labeled FAP^+ GNS cell lines
163 with a fluorescent dye (CellTrace Far Red; CTFR) and mixed them with unlabeled GNS cells
164 lacking FAP expression. This target-cell mixture was incubated with FAP-CAR-T cells or NT-T
165 cells for 48 hours and the viability of each target-cell population analyzed by flow cytometry
166 (see Supplementary Figure 2 for an overview of the experimental design). Two different pairs
167 of FAP^+/FAP^- GNS cell lines were used. Pair 1 consisted of FAP^+ MN1 cells with FAP^- RKI1 cells,
168 and Pair 2 consisted of FAP^+ CCB-G3-C cells with FAP^- SJH1 cells. Whereas MN1 and CCB-G3-C
169 cells showed uniform expression of FAP by flow cytometry (see Figure 2b), RKI1 and SJH1 cells
170 lacked any detectable surface expression (Figure 3a). These FAP-negative GNS cells also lacked
171 significant gene expression by microarray analysis (data not shown).

172 An example of the gating strategy and analysis of the FAP$^-$ target cell fraction is shown in
173 Figure 3b, while pooled data are summarized in Figure 3(c-d). As expected, FAP-CAR-T cells
174 induced efficient killing of FAP$^+$ target cells (Fig 3c, and representative data in Supplementary
175 Figure 3). Also as expected, the viability of FAP$^-$ tumor cells cultured alone was not affected by
176 incubation with FAP-CAR-T cells, thereby ruling out off-target effects. But when FAP$^-$ target
177 cells were mixed with FAP$^+$ target cells and incubated with FAP-CAR-T cells, significant killing
178 of the FAP$^-$ tumor cells was observed (Figure 3b and d). Thus, FAP-CAR-T cells can exert
179 substantial bystander killing of tumor cells lacking FAP, but only once they have been
180 activated by cells expressing their cognate antigen. To determine if the bystander killing effect
181 is unique to FAP-CAR-T cells, we also tested GD2-specific CAR-T cells on two GNS cells
182 expressing low levels of GD2 (16-26% GD2-positive). Real-time cytotoxicity assays revealed
183 complete lysis of these target cells despite heterogeneous antigen expression (Supplementary
184 Figure 4), thus suggesting that the bystander killing activity of CAR-T cells is not restricted to a
185 particular CAR.

186

187 **Bystander cytotoxicity occurs independently of Fas/FasL but can be mediated by soluble**
188 **factors**

189 Bystander killing of antigen-negative targets has recently been reported to occur via Fas-FasL
190 interactions[27]. To determine if this molecular axis was at play in our system, we first
191 investigated expression of Fas on our GNS cell lines, and expression of FasL on our FAP-CAR-T
192 cells. Although variable levels of Fas were detected on the GNS cell lines (RKI1, SJH1 and CCB-
193 G6-T) found to be susceptible to bystander killing (Supplementary Figure 5a), there was

194 almost no expression of FasL by FAP-CAR-T cells, even after co-culture with FAP^+ target cells
195 and with permeabilization to detect intracellular stores of FasL (Supplementary Figure 5b).
196 Soluble FasL in culture medium was also low (< 20 pg mL^{-1}, data not shown). ZB4 was reported
197 as a function-blocking anti-Fas antibody[28]. We confirmed this in our soluble FasL induced
198 cytotoxicity assay (Supplementary Figure 5c). However, ZB4 failed to attenuate either direct
199 killing (data not shown) or bystander killing (Supplementary Figure 5d-e). We therefore
200 conclude that bystander killing is unlikely to be mediated by Fas/FasL interactions in our
201 system.

202 We next hypothesized that soluble factors such as cytokines could contribute to the bystander
203 killing effect. This was tested by separating antigen-negative target cells from CAR-T cells
204 using a semi-permeable membrane. FAP-CAR-T or NT-T cells were seeded together with FAP^+
205 GNS cells in the lower chambers of Transwell assemblies, while FAP^- GNS cells were seeded in
206 the upper chambers (Figure 4a). After 48 hours, cells in the upper chambers were stained
207 using propidium iodide (PI) to label dead cells and Hoechst 33342 to visualize total nuclei, and
208 cell viability calculated by the ratio of PI/Hoechst-stained cells. The same combinations of FAP^-
209 SJH-1/FAP^+ CCB-G3-C cells and FAP^- RKI-1/FAP^+ MN-1 cells from Figure 3 were used in this
210 assay. In keeping with our hypothesis, significant killing of FAP^- tumor cells in the upper
211 chamber (SJH-1 or RKI-1) was observed when FAP-CAR-T cells were present in the lower
212 chamber together with FAP^+ tumor cells (Figure 4b-d).

213 Since the Transwell experiments suggested that bystander killing of antigen-negative cells can
214 be at least partly mediated by soluble factors, a panel of cytokines and cytotoxic proteins was
215 measured in co-culture supernatants using a multiplexed flow cytometric bead assay. Large

216 amounts of TNF-α, IFN-γ, granzyme A, granzyme B and granulysin were released when FAP-
217 CAR-T cells were co-cultured with FAP^+ GNS cells, but not when cultured alone (Figure 4e).
218 Perforin was also detected in the co-culture supernatants but was similarly secreted in the
219 absence of target cells, suggesting constitutive secretion by FAP-CAR-T cells. As expected, the
220 NT-T cells generally secreted only low levels of these factors, even in the presence of FAP^+
221 GNS tumor cells. Together, our results indicate that FAP-CAR-T cells can be activated by
222 antigen to secrete a range of cytotoxic cytokines and proteins, which may contribute to the
223 contact-independent bystander killing observed in the Transwell system.

224

225 **FAP-CAR-T cell activation mobilizes the CAR-negative T-cell fraction to enhance cytotoxicity**

226 It has long been recognized that, in addition to antigen-dependent cytotoxicity, T cells can
227 also undergo cytokine-induced bystander activation [29]. Our FAP-CAR-T cell products contain
228 ~75% CAR-negative T cells, leading us to hypothesize that CAR-T cells may secrete cytokines to
229 mobilize the non-transduced T cells into the antitumor response after activation by FAP-
230 expressing tumor cells (Figure 5a). In this way, the whole population of T cells could be
231 synchronized to exert cytotoxicity against both antigen-positive and antigen-negative tumor
232 cells. Cytokines including IL-2, IL-12, IL-15 and IL-21 have been reported to initiate antigen
233 nonspecific T-cell activation[30-32]. And although IL-15 and IL-12 are primarily produced by
234 antigen presenting cells, IL-2 and IL-21 can be produced by T cells. We showed that IL-2 was
235 secreted by FAP-CAR-T cells after antigen activation (Figure 1d), suggesting that it could be
236 one of the cytokines to mobilize normal T cells during bystander killing.

237 We performed additional real-time cytotoxicity assays to explore these concepts by
238 recapitulating the bystander activation and killing processes *in vitro*. The cytotoxicity of FAP-
239 CAR-T cells or NT-T cells was tested against MN1 GNS cells expressing moderate levels of FAP,
240 with or without the addition of 20ng/ml exogenous IL-2 (Figure 5b). FAP-CAR-T cells displayed
241 strong cytotoxicity against MN1 as expected, which was further boosted by the addition of IL-
242 2. This effect was marginal at high E:T ratios but became more pronounced at lower E:T ratios
243 as CAR-expressing effector cells became limiting. Of note, IL-2 also dramatically increased the
244 cytotoxicity of control T cells. For example, at a high (5:1) E:T ratio, NT-T cells supplemented
245 with IL-2 induced as much tumor cell killing as FAP-CAR-T cells. This observation supports the
246 concept that, although IL-2 may also boost the activity of antigen-activated CAR^+ cells, it has
247 the greatest impact on the non-transduced 'bystander' cells.

248 We further analyzed cytokines and cytotoxic proteins in supernatant samples collected from
249 these assays. In addition to IL-2, we measured another 11 analytes (Figure 5c, Supplementary
250 Figure 6, Table 1). The addition of IL-2 to NT-T cells significantly increased the levels of all
251 factors except IL-10 and IL-17a (see column 3 in Table 1), suggesting that these two cytokines
252 were upregulated only by CAR stimulation, not IL-2. Furthermore, by comparing NT-T cells +
253 IL-2 to CAR-T cells + IL-2, we could show that all factors were further boosted by CAR
254 engagement except for perforin (see column 4 in Table 1), suggesting that IL-2 alone was
255 sufficient to induce maximum secretion of soluble perforin. Interestingly, all analytes showed
256 a positive correlation with the extent of cytotoxicity except soluble Fas and FasL (Table 1,
257 column 2). These results agree with those from our ZB4 blocking experiment (Supplementary

258 Figure 5), which did not support a significant role for the Fas/FasL axis in cytotoxicity in our

259 system.

Cytokine	Correlation with cytotoxicity Adj-R2	*P*-value	IL-2/N-T vs N-T (Significant or not)	IL-2/N-T vs IL-2/FAP-CAR-T (Significant or not)
Granzyme B	0.47994	8.66E-07	Yes	Yes
IL-4	0.43468	4.06E-06	Yes	Yes
IFN γ	0.43145	4.51E-06	Yes	Yes
Perforin	0.29523	2.52E-04	Yes	**No**
IL-6	0.26234	5.99E-04	Yes	Yes
TNFα	0.25307	7.60E-04	Yes	Yes
IL-10	0.22098	0.00171	**No**	Yes
IL-17a	0.20964	0.00226	**No**	Yes
Granulysin	0.14905	0.00962	Yes	Yes
sFas	-0.02626	**0.81865**	Yes	Yes
sFas L	-0.02713	**0.88065**	Yes	Yes

260 **Table 1**. Linear fitting regression was performed using cytolysis $\%_{36h}$ vs cytokine concentration

261 $_{(pg\ mL^{-1})}$. The cytokines were ranked by their adjusted R^2 value from high to low in the table. *P*-

262 value was calculated by ANOVA. The significance of differences between NT-T ± IL-2 or

263 between NT-T and FAP-CAR-T was determined by paired *t*-test. $P < 0.05$ was considered

264 significant.

265 In summary, our findings suggest that cytokines, such as IL-2 used here, can stimulate the

266 non-transduced fraction of a CAR-T cell product also to mediate tumor cell killing.

267 Furthermore, this amplification of the response may be an important aspect of the bystander

268 killing mechanism, because IL-2 also resulted in upregulated secretion of factors such as TNFα,

269 IFNγ, granzyme and granulysin, which are candidate mediators of bystander killing. Other

270 cytokines upregulated in this system (IL-4, IL-6, IL-10, and IL-17) are not directly involved in

271 cytotoxicity but can support T- and B-cell function.

272

273 **FAP-CAR-T cells exhibit a lack of toxicity against healthy cells and control the growth of**
274 **tumors in a subcutaneous glioblastoma xenograft model despite heterogeneous antigen**
275 **expression.**

276 To assess the function of our CAR-T cells *in vivo*, we tested their ability to control the growth
277 of subcutaneous human xenograft tumors in immunodeficient (NSG) mice. Glioblastoma is
278 well-known for its cellular heterogeneity, and we have shown that expression of FAP by
279 glioblastoma tumor cells is also heterogenous [21]. Accordingly, we generated a model with
280 mixed FAP^+ and FAP^- tumor cells. FAP^+ U87 cells were engineered to express RFP, while FAP^-
281 U251 cells were engineered to express GFP, to allow monitoring of the mixed tumor cell
282 populations. In an initial *in vitro* assay, the single target cell populations or the target cell
283 mixture were co-cultured with FAP-CAR-T cells or NT-T cells and surviving cells were counted
284 using fluorescence microscopy 24 hours later. Counts of FAP^- U251 cells were reduced
285 significantly only when co-cultured with both U87 cells and FAP-CAR-T cells (Figure 6a),
286 suggesting that antigen-negative U251 tumor cells are also susceptible to bystander killing
287 from FAP-CAR-T cells, similar to our earlier observations using GNS cells. Thus, in addition to
288 replicating the heterogeneous nature of glioblastoma tumors, a mixed U87/U251 tumor
289 model also seems suitable to examine the bystander killing capacity of FAP-CAR-T cells *in vivo*.

290 Another important consideration before proceeding to animal studies was safety. We needed
291 to determine whether bystander killing would result in off-target toxicity by targeting normal
292 cells. To address this concern, we conducted a four-way co-culture experiment. Primary
293 human Endothelial Colony Forming Cells (ECFCs), derived from circulating progenitor cells in

294 peripheral blood, serve as a model for healthy blood vessels[33], and as shown in
295 Supplementary Figure 7, express minimal FAP protein in their surface. We co-cultured ECFCs
296 with U87 and U251 cells and subsequently treated the cell mixture with effector cells (either
297 FAP-CAR-T or NT-T cells), then 48 hours later flow cytometry was used to assess relative
298 numbers of the various target cell populations (Figure 6b). As expected, FAP-CAR-T cells killed
299 the FAP^+ U87 cells. The FAP^- U251 cells were also killed, in keeping with bystander killing
300 activity. However, ECFCs in the same culture well were not targeted, suggesting that the key
301 bystander killing mechanisms at play in this system only target malignant cells.

302 The fluorescently tagged U87 and U251 cell lines were mixed at a 2:1 ratio, respectively,
303 before subcutaneous implantation in each flank of NSG mice. The 2:1 mixing ratio was
304 selected after an initial pilot study and resulted in the most evenly balanced tumors at
305 endpoint (Figure 6c, Supplementary Figure 8 a-b). Compared to either NT-T cells or no
306 treatment, intravenous administration of a low dose (1×10^6) of FAP-CAR-T cells significantly
307 reduced tumor growth (adjusted $P < 0.0001$ by Type II ANOVA for both control comparisons;
308 Figure 6d), and significantly increased survival time of treated mice (both $P < 0.0001$ by Log-
309 Rank test; Figure 6e). Notably, the FAP-CAR-T cells did not induce any overt signs of toxicity,
310 with no mice needing to be culled due to weight loss, signs of distress/illness, or poor body
311 condition. In mice treated with FAP-CAR-T cells, both the GFP and RFP signals in necropsied
312 tumor tissues were significantly reduced compared to tumors in either control group (Figure
313 6f), suggesting CAR-T cell targeting of both FAP^+ U87-RFP and FAP^- U251-GFP cells. These
314 findings support the effectiveness of our FAP-CAR-T cells in controlling the growth of
315 glioblastoma cells *in vivo*, even in the face of heterogeneous expression of target antigen.

316 **DISCUSSION**

317 For many years, FAP has been recognized as a promising immunotherapy target for
318 carcinomas and mesothelioma [14-17, 19, 20]. More recently, we have proposed FAP as a candidate
319 immunotherapy target antigen for glioblastoma [21]. Studies from our group and others have
320 shown that, in glioblastoma, FAP is heterogeneously expressed on tumor cells themselves, but
321 more consistently by tumor-supporting stromal populations including endothelial cells and
322 pericytes. This sits in sharp contrast to the limited expression in healthy tissues and vessels [21,
323 34]. Despite all these characteristics, until now FAP has never been tested as a target antigen
324 for immunotherapeutic strategies in glioblastoma.

325 Glioblastoma has striking intra-tumor heterogeneity [35]. For initial confirmation of targeting
326 specificity, we used long-term cell lines including U87 and U251, and these studies
327 successfully demonstrated that our FAP-CAR-T cells secrete IL-2 and induce cytolysis only
328 when FAP is expressed. However, these cell lines (which have been cultured for many decades
329 *in vitro* in the presence of xenogeneic serum) may lose multipotency, develop pro-survival
330 mechanisms and fail to model the disease properly [36]. For further *in vitro* testing, we therefore
331 moved to the use of glioma neural stem (GNS) cell lines, which are patient glioblastoma
332 tissue-derived cells expanded under serum-free conditions to a limited passage number
333 (generally < 30) and maintain a more *in vivo*-like phenotype [21, 37]. Our group has developed a
334 panel of GNS cells from patient samples and characterized them for FAP expression [21] and we
335 used these GNS cells, together with those from the Q-Cell resource [38] as *in vitro* models to
336 investigate more authentically how our CAR-T cells tackle the heterogeneity of glioblastoma,
337 including low and heterogeneous patterns of FAP expression.

338 Our results using GNS cells in a sensitive real-time cytotoxicity assay indicated that the
339 percentage of cells lysed by FAP-CAR-T cells can greatly exceed the percentage of target cells
340 expressing the antigen. Further flow cytometry-based analysis of co-cultured GNS cells
341 confirmed that FAP-CAR-T cells can kill antigen-negative tumor cells, but only in the presence
342 of antigen-positive tumor cells. Antigen/epitope spreading is a phenomenon whereby
343 immune reactivity is broadened following the release of antigens during chronic inflammation,
344 and is dependent on an intact immune system and the involvement of antigen-presenting
345 cells (APCs)[39]. It is highly unlikely that this phenomenon occurs in the reductionist co-culture
346 systems used here. Rather, we conclude that FAP-CAR-T cells are capable of 'bystander' killing,
347 a phenomenon long recognized in T-cell immunology but poorly understood [40, 41]. The
348 significance of bystander killing in CAR-T cell function is also just beginning to be appreciated
349 [27, 42], and many questions remain. For example, it is unclear whether all CAR-T cell products
350 have bystander killing capacity, or does this depend on factors such as CAR structure or target
351 cell susceptibility? Based on our observations using CAR T cells targeting FAP or GD2, we
352 believe that this function may be a common feature of CAR-T function that has been generally
353 underappreciated in the field because it will not be revealed in such short-term cytotoxicity
354 assays as the classical chromium release assay. By using the novel Maestro Z instrument to
355 track target cell destruction over several days, we allow CAR-T cells the time required to be
356 activated by CAR engagement and then deploy a range of cytotoxic mechanisms against
357 antigen-negative tumor cells. Therefore, it is possible that all CAR-T cell products can perform
358 bystander killing to some degree, but a sufficient observation period is required to record this
359 phenomenon.

360 Another important question regarding bystander killing is: what are the key effector
361 molecules? The major killing mechanism described for CAR-T cells has been direct cytolysis,
362 which is induced by perforin and granzyme and delivered via a CAR-mediated immunologic
363 synapse [43]. Recent studies have suggested that the Fas/FasL signaling axis participates in CAR-
364 T cell cytotoxicity, and also in bystander killing [27, 42]. In contrast, we did not find evidence that
365 Fas/FasL contributes to bystander killing (or cytotoxicity in general) by FAP-CAR T cells. We did,
366 however, observe that the bystander killing effect was at least partly mediated by soluble
367 factors, as significant cytotoxicity was observed even when the CAR-T cells and tumor cells
368 were not in direct contact. Determining exactly which secreted factor or factors drive
369 bystander killing by FAP-CAR-T cells is beyond the scope of the present study. However, we
370 did detect secretion of a range of cytokines and cytotoxic granule components upon antigen
371 engagement of FAP-CAR-T cells. Two cytokines of particular interest are TNFα and IFNγ, both
372 of which have a direct antitumor effect [44, 45]. Moreover, TNF has previously been shown to
373 play a critical role in the antitumor activity of HER2-targeting CAR-T cells, and to facilitate
374 bystander killing in the context of patient-derived colorectal tumoroids[46]. In this system, the
375 relatively low penetrance of HER2-CAR-T cells meant that effective cytotoxicity could only be
376 achieved with a diffusible factor such as TNF. We also detected secretion of surprisingly high
377 levels of molecules such as granzyme B and perforin, which are normally involved in
378 cytotoxicity mediated by immunologic synapse formation. Whether these molecules mediate
379 cytotoxicity when secreted into the surrounding environment is unclear. In addition to soluble
380 cytokines, classic innate-like effector molecules such as NKG2D could also potentially
381 contribute to bystander killing (33). Indeed, initial experiments suggested that NKG2D could
382 be induced on FAP-CAR-T cells following antigen engagement (data not shown). It is likely that

383 bystander killing by CAR-T cells is complicated and multifactorial, with the contribution of
384 different effector mechanisms varying according to such factors as the tumor type, the CAR-T
385 cell phenotype and the susceptibility of individual target cells. Further research is warranted
386 to better understand these mechanisms and how they are regulated. Indeed, if bystander
387 killing can be optimized, uniform target antigen expression may not be required for efficient
388 and complete tumor destruction by CAR-T cells. The potential of this approach has recently
389 been observed using inhibitor of apoptosis protein (IAP) antagonists to facilitate antigen
390 nonspecific killing by CAR-T cells targeting EGFRvIII [47].

391 The fact that bystander killing does not rely on antigen-directed targeting raises questions of
392 safety, because there is a theoretical risk of targeting healthy cells and tissues. However, no
393 overt toxicity was induced by FAP-CAR-T cells in our mouse xenograft model, even though the
394 MO38 scFV has been shown to cross-react with murine FAP[24]. Moreover, co-culture
395 experiments demonstrated that FAP-CAR-T cells can induce specific targeting of FAP^+ tumor
396 cells and bystander killing of FAP^- tumor cells while sparing non-malignant ECFCs within the
397 same culture well. Together, these observations suggest that the bystander killing effector
398 mechanisms operative in FAP-CAR-T cells may only be effective against cancer cells that
399 express cognate receptors, whereas healthy cells lacking receptor expression are not targeted.

400 A typical CAR-T cell product contains both virally transduced (CAR-expressing) T cells and a
401 variable proportion of non-transduced T cells. Here, we postulate that the non-transduced
402 fraction of a CAR-T cell product can significantly contribute to killing of both antigen-positive
403 and antigen-negative tumor cells through the process of bystander activation'. This involves
404 activation of T cells in a T-cell receptor-independent and cytokine-dependent manner, and has

405 long been observed during viral and bacterial infection[48, 49], as well as in anti-tumor immunity
406 [29]. IL-18 and IL-15 are important factors that induce bystander activation of T cells [50], and IL-2
407 and IL-15 can convert T cells to lymphokine-activated killer (LAK) cells which exert cytotoxicity
408 through antigen-independent mechanisms[31, 32].

409 Of particular interest is IL-2, which was the first cytokine approved for human cancer therapy
410 [51]. IL-2 is a master cytokine which shapes the proliferation, differentiation and function of T
411 cells and which can regulate the cytolytic machinery of T cells, including upregulation of
412 perforin, granzymes and other proteins required for cytolytic granule fusion [52]. In this study,
413 we hypothesize that when stimulated by antigen, CAR-T cells can produce cytokines such as
414 IL-2, which will induce the non-transduced T cells to exert cytotoxicity via antigen-
415 independent mechanisms. Our observation of enhanced *in vitro* cytotoxicity achieved by
416 supplementing with additional IL-2 may not appear novel on its own. However, this specific
417 experiment offers us the opportunity to analyze various cytokines obtained from the assay
418 and establish a correlation between cytokines and cytotoxicity. From this analysis, we have
419 been able to determine which cytokines are likely to contribute to bystander killing and which
420 are unlikely to do so (Figure 5c and Table 1). This IL-2-dependent function has the potential to
421 broaden the antitumor effect of CAR-T products.

422 To mimic the heterogeneity of glioblastoma *in vivo*, we developed a mixed tumor model in
423 which fluorescently tagged U87 and U251 cells were combined in an optimized ratio to
424 produce tumors that had both cell types still present at endpoint. Using this model, we have
425 shown that FAP-CAR-T cells can significantly delay tumor growth and extend survival, despite
426 antigen heterogeneity. Complete tumor destruction was not observed in these experimental

427 conditions, but it is worth noting that we used a low dose of CAR-T cells (1×10^6) with
428 relatively low transduction efficiency (~25%) administered in a single intravenous dose. In
429 future studies, a higher CAR-T cell dose with greater transduction efficiency may yield more
430 complete tumor control. Analysis of tumor tissues at endpoint revealed that both U87 FAP^+
431 and U251 FAP^- cells were reduced following FAP-CAR-T cell treatment, suggesting that the
432 CAR-T cells exert longitudinal control over both U251 and U87 cells, in keeping with our *in*
433 *vitro* findings of bystander killing. In these tumors, there were large areas of non-fluorescent
434 tissue, constituting 90% of the area in the FAP-CAR-T treated group, 65% in the NT-T group,
435 and 50% in the untreated group. These non-fluorescent cells may come from two sources:
436 nonfluorescent tumor cells that finally escape immune control or infiltrating mouse-derived
437 stromal cells such as fibroblasts and macrophages [53].

438 Our observations suggest that bystander killing mechanisms may enable CAR-T cells to target
439 more tumor cells than would be predicted from the target antigen expression pattern, and
440 thus may contribute to tumor destruction even in the presence of tumor heterogeneity.
441 Approaches to boost endogenous bystander killing pathways may therefore increase the
442 potency of CAR-T cell therapies, although the benefits of such approaches must be balanced
443 against the theoretical risk of off-tumor toxicity. However, receptors such as NKG2D and even
444 secreted cytokines are expected to act in a highly localized fashion. It was estimated, for
445 example, that under physiologic conditions in dense tissues such as lymph nodes, the cytokine
446 IL-2, interacts over a characteristic length scale of 8-14 cell diameters (80-140 µm), which is
447 determined by a balance between diffusion and consumption of cytokine [54]. Therefore, we
448 might expect that bystander killing effects, may be limited to the tumor microenvironment
449 where CAR-T cells engage with antigen.

450 In this study, we have developed a novel FAP-targeting CAR and shown, for the first time, that
451 FAP-CAR-T cells effectively destroy glioblastoma cells *in vitro* and *in vivo*. These findings help
452 to address the critical need for new and better target antigens for CAR-T cell therapy in the
453 setting of glioblastoma. In addition, we highlight two mechanisms that broaden the antitumor
454 effect of our CAR-T cell product: bystander killing of antigen-negative tumor cells, and
455 cytokine-mediated bystander T-cell activation. Future work to better understand these
456 mechanisms may reveal opportunities to enhance CAR-T cell function and promote more
457 effective clearance of heterogenous solid tumors, a strategy that may be further augmented
458 by multi-antigen targeting.
459

460 **METHODS**

461 **Tumor cell lines**

462 Long-term cell lines and GNS cells used in this study are listed in Supplementary Table 1.
463 Short-term cultured GNS cell lines were a kind gift from Professor Bryan Day (QIMR Berghofer
464 Medical Research Institute, Brisbane, Australia) or were generated in our laboratory as
465 described[21, 55]. U251, U87 and RPMI-7951 cell lines were obtained from ATCC. U251-GFP and
466 U87-RFP cells were generated via lentiviral transduction of parental cell lines with the
467 lentiviral vectors pBLIV-MSCV-GFP-T2A-Fluc and pBLIV-CMV-RFP-T2A-Fluc (System Biosciences
468 Inc, Palo Alto, USA), respectively. GFP- or RFP-expressing cells were sorted using MoFlo Astrios
469 Cell Sorter (Beckman Coulter, Brea, USA). U251 and U87 (and their GFP/RFP-labelled variants)
470 were maintained in Minimum Essential Medium Eagle supplemented with 10% fetal bovine
471 serum (FBS), 1% penicillin/streptomycin, 1% glutamax, 1% sodium pyruvate, and 1% MEM

472 non-essential amino acid solution (all Thermo Fisher Scientific, Scoresby, Australia). RPMI-
473 7951 cells were maintained in RPMI-1640 medium supplemented with 10% fetal bovine
474 serum (FBS), 1% penicillin/streptomycin and 1% glutamax. GNS cell lines were cultured in
475 StemPro Neural Stem Cell medium (StemPro NSC, Thermo Fisher Scientific) in flasks, which
476 were pre-coated with Matrigel (Corning, Silverwater, Australia) diluted 1/100 in PBS according
477 to the manufacturer's recommendations. Cultures were passaged using Accutase (Thermo
478 Fisher) when they reached ~70-90% confluence.

479

480 **CAR transgene design and generation of CAR-T cells**

481 Anti-FAP scFv with Myc tag was obtained by PCR using donated plasmid containing MO36 as a
482 template. The primers were F: GCCCGACGTCGCCACCATGGACTGGATCTGGCGCATC; R:
483 TGCGGCCCCATTCAGATCCTCTTCTGAGATGAGTTTTTGTTCTGCGGCCGCCCGTTTTATTTCCAGC. A
484 human IgG4 hinge/CH2CH3 was chosen as a long spacer to reduce the affinity to human
485 FcRs[56, 57]. Aiming to avoid activation-induced cell death by further reducing its affinity to
486 human and murine FcRs, additional modifications were made to the CH2 region. Three amino
487 acid (PVA) derived from IgG2 substituted for four amino acids (EFLG) in the corresponding
488 region of IgG4, and another glycosylation motif was mutated from N to Q[58, 59]. The CD3ζ and
489 CD28 signaling domains were positioned after the spacer. Hinge, spacer and signaling domains
490 were synthesized by GeneArt (Thermo Fisher). All fragments were assembled on pEntry vector
491 and subcloned into lenti vector pPHLV-A.

492 The lentivirus encoding FAP-CAR was generated in HEK293T cells through transfection.
493 HEK293T cells in a T175 flask were transfected with 46.4µg DNA consisting of equal amounts

494 of four plasmids using 138µL lipofectamine 2000 (Thermo Fisher). The plasmids were: (i)
495 pHLVA-FAP-CAR, which provides the lentiviral RNA containing the CAR (described in previous
496 section); (ii) pMD2.G, which provides expression of VSV-G; (iii) pMDLgpRRE, which provides
497 expression of gag pol; and (iv) pRSV-REV which provides the rev gene for lentiviral packaging.
498 The supernatant was harvested 48h after transfection, centrifuged at 500 x *g* for 10min. and
499 filtered through a 0.45µm filter (Nalgene Rapid-Flow™, Thermo Fisher), ready for transduction.
500 To produce CAR-T cells, a 24-well plate was pre-coated with anti-CD3 (OKT3) and anti-CD28
501 antibodies (15E8) (Miltenyi Biotec, Macquarie Park, Australia) at 1µg mL^{-1} on day 0. PBMC
502 were seeded at 1×10^6 cells/well on day 1 in Advanced RPMI (Thermo Fisher) with 10% FBS,
503 with IL-7 and IL-15 (Miltenyi) added at 10 ng mL^{-1} and 5 ng mL^{-1}, respectively, on day 2. On day
504 3, the activated T cells were transduced by spinoculation with lentivirus encoding FAP-CAR. In
505 brief, 0.5mL T cells at 2×10^6 cells mL^{-1} were mixed with 1.5mL lentiviral supernatant and
506 centrifuged in 24-well plates pre-coated with 7 µg mL^{-1} Retronectin (Takara Bio, San Jose, USA)
507 at 1000 x *g* for 20min. The transduced T cells were expanded for another 4 days with IL-7/IL-
508 15 before cryopreserving in FBS + 10% DMSO and storage in liquid nitrogen. Before use, the
509 CAR-T cells were thawed and rested overnight in Advanced RPMI with 10% FBS. CAR
510 expression was detected by FITC-conjugated anti-Myc tag antibody (Abcam, Melbourne,
511 Australia) and analyzed by flow cytometry using an Accuri C6 Plus flow cytometer (BD
512 Biosciences, Macquarie Park, Australia).

513

514 **Flow cytometry analysis of FAP expression**

515 U251, U87 and RPMI-7951 cells were stained by PE-conjugated anti-FAP antibody (clone
516 427819, R&D Systems) in 5% BSA/PBS staining buffer for 30min. Cells were washed with
517 staining buffer and 1µL 7AAD (Thermo Fisher) was added in a final resuspension volume of
518 200µL before analysis by flow cytometry (BD Accuri™). For staining of GNS cultures, cells were
519 harvested using Accutase (Thermo Fisher), washed in PBS and resuspended in FACS buffer
520 (PBS + 1% bovine serum albumin + 0.04% sodium azide). Cells were then stained as described
521 above.

522

523 **T-Cell Phenotype:**

524 T cells were resuspended in 200µL of FACs buffer at a concentration of 2×10^6 cells mL^{-1}.
525 Human Fc block (BD) was added (2µL per sample) and incubated for 5min on ice, then samples
526 were centrifuged at 300 × g for 5min and the pellets resuspended in 50µL of FACs buffer.
527 Samples were stained for 30min on ice using the following antibodies: anti-CD3-PE (BD), anti-
528 CD4 BV510 (BD), anti-CD8 PE-Cy7 (BD), anti-CD45RA APC (BD), anti-CCR7 (CD197) BV421 (BD),
529 anti-Myc AF488 (Abcam). Samples were washed twice with FACs buffer before analysis by
530 flow cytometry using the Accuri C6 Plus, as per above.

531

532 **Cytotoxicity assays**

533 Four different cytotoxicity assays were used to address different biologic questions.

534 *Cytotoxicity assay using real-time impedance-based cell analysis*

535 The Axion BioSystems (Atlanta, USA) Maestro Z system was used to measure cytotoxicity.
536 After addition of 100µL of culture medium to the CytoView-Z plate (Axion Biosystems), a
537 baseline reading was taken and then target cells were seeded in a volume of 100µL at 15,000
538 cells/well for U87 and U251 or 10,000 cells/well for GNS cultures. The wells were pre-coated
539 with Matrigel if GNS cells were used as targets. Resistance values were monitored every 60sec
540 using AxisZ software during overnight culture at 37°C in the Maestro Z instrument. Once
541 formation of a stable monolayer was confirmed, 100µL of CAR-T cells were added in the same
542 medium as the target cells. Resistance values were normalized to a time shortly after adding
543 CAR-T cells once readings had re-stabilized. Cytotoxicity was measured as %lysis based on the
544 impedance ratio of tested cells and untreated control cells, which was calculated by AxisZ
545 software.

546 *Cytotoxicity assay by flow cytometry*

547 GNS cells (1×10^5) were co-cultured with an equal number of FAP-CAR-T cells or control non-
548 transduced T cells (NT-T) in equivalent culture conditions in StemPro NSC medium in a 24-well
549 plate. In co-cultures of pairs of GNS cell lines of differing levels of FAP expression, FAP-
550 expressing GNS cells were first pre-labeled with CellTrace™ Far Red (CTFR; Thermo Fisher) at
551 1µM for 20min at 37^0C, to differentiate the populations, and equal numbers of FAP^+ and FAP^-
552 cells were mixed. After 48 hours, T cell suspension were collected and adhered tumour cells
553 were detached and harvested using StemPro™ Accutase™ (Thermo Fisher). T cells and tumor
554 cells were pooled together and collected by centrifugation. Cells were stained in PBS with
555 Fixable Viability Stain 575V (BD) or Fixable Viability Dye eFluor™ 506 (Invitrogen) where
556 indicated for 10min at room temperature, before antibody staining. The antibodies used for

557 staining included: BB515 anti-Fas (clone DX2, BD Biosciences), BV786 anti-CD3 (clone SK7, BD
558 Biosciences), PE anti-FAP (clone 427819, R&D Systems) and BV480 anti-FasL (clone NOK-1, BD
559 Biosciences). Samples were acquired on an LSR Fortessa (BD Biosciences) and data analyzed
560 using FCS Express 7 Cytometry (De Novo software, Pasadena, CA, USA).

561 *Cytotoxicity assay to assess the role of soluble factors*

562 These experiments were conducted in 24-well Transwell plates (Corning) or Nunc Cell Culture
563 Inserts (Thermo Fisher) with a 0.4µm pore size. FAP-expressing cells were plated in the lower
564 well at 1 x 10^5 cells/well, and 1 x 10^4 FAP-negative cells were seeded in the upper inserts.
565 When monolayers of target cells had established, FAP-CAR-T cells or non-transduced T cells
566 were added to the bottom well at a 1:1 E:T ratio. After 48h incubation at 37°C, cells in the
567 inserts were stained using propidium iodide (PI) (Thermo Fisher) at 1 µg mL^{-1} and Hoechst
568 33342 (Thermo Fisher) at 2µM for 20min at 37°C. Without washing, inserts were imaged using
569 an IX73 microscope equipped with CoolLED pE-4000 light source and running CellSens
570 software (Olympus). The cells on each image were counted by QuPath (University of
571 Edinburgh). Cell viability was calculated as [1 - (PI counts/Hoechst counts)] x 100%.

572 *Cytotoxicity assay using fluorescence imaging of U87-RFP and U251-GFP cells*

573 U87-RFP and U251-GFP were seeded with starting numbers of 5× 10^4 cells/well. FAP-CAR-T
574 cells were immediately added at a 1:1 E:T ratio. The cocultured cells were imaged by the
575 Olympus IX73 microscope 24h later using 100ms exposure for RFP and 3ms exposure for GFP.
576 Three fields of views were taken from each well and duplicate wells were used for one assay.
577 The images were analyzed by ImageJ for fluorescence counts using threshold values of 68-255

578 for RFP and 98-255 for GFP. All images were collected and analyzed using the same
579 parameters for consistency.

580 *Endothelial Colony Forming Cell (ECFC) co-culture experiments*

581 Endothelial colony-forming cells (ECFCs) were derived from peripheral blood obtained from
582 healthy human donors, following established protocols[60, 61]. Briefly, peripheral blood
583 mononuclear cells were plated on collagen I (Corning) -coated 48 well plates in EGM-2
584 medium (Lonza, Switzerland), supplemented with 20% ES cell-screened FBS (Hyclone, GE
585 Healthcare, Chicago, USA) until colonies formed. Cells were passaged and maintained for no
586 more than nine passages in EGM-2 medium with 20% FBS, with confirmation of ECFC markers
587 using flow cytometry. A mixed target cell population consisting of ECFCs, U87-RFP, and U251-
588 GFP cells (1.5 X 10^5 each) was co-cultured for 48 hours in EGM-2 medium with 6 X 10^5 effector
589 cells in 24-well plates. Subsequently, the cells were washed, treated with trypsin, harvested in
590 1.5 mL PBS, and analyzed using an Accuri C6 Plus flow cytometer. From each sample, cells
591 from a fixed volume of 66 µL were counted. U87-RFP and U251-GFP cells were counted based
592 on fluorescent gating, while ECFCs were identified through their lack of fluorescence. The cell
593 counts obtained after 48 hours were compared with those from samples collected at 0 hours
594 to determine the fold change.

595

596 **Measurement of secreted factors**

597 To measure IL-2 secretion, target cells were seeded in a flat-bottom 96-well plate at 20,000
598 cells/well on day 0. On day 1, 1×10^5 CAR-T cells were added per well. The supernatant was

599 collected on day 3 and analyzed by human IL-2 ELISA Kit (Thermo Fisher) according to the
600 manufacturer's protocol.

601 To measure levels of 13 soluble factors simultaneously using the LEGENDplex Human CD8/NK
602 Panel (BioLegend, San Diego, USA), supernatants were collected from cytotoxicity assays
603 conducted in the Maestro Z instrument at endpoint and stored at -20°C. Assays were
604 conducted according to the manufacturer's protocol and analyzed using a BD LSR Fortessa.

605

606 **Murine subcutaneous tumor xenograft model**

607 Animal experiments were approved by the University of South Australia Animal Ethics
608 Committee (Ethics number: 45/17). Female nonobese diabetic/severe combined
609 immunodeficiency/IL2Rγ-null (NSG) mice were purchased at 6 weeks from the Animal
610 Resource Centre (Perth, Australia) and housed in the Immunocompromised Suite of the Core
611 Animal Facility of the University of South Australia in isolator cages. Mice were provided with
612 standard chow and sterile water *at libitum*, and given soaked food and sunflower seeds as
613 required to support weight maintenance. At least 2 weeks were allowed for acclimatization
614 prior to initiating experiments. Sample size for treatment and control groups was calculated *a*
615 *priori* based on f = 0.40, SD = 0.2, power level 0.9 for the primary outcome measure of tumor
616 volume. Mice were randomly allocated to groupings (n = 4-5 per cage) at the beginning of the
617 experiment; no blinding was performed. To minimize potential confounders, animals were
618 housed in adjacent cages under the same conditions (lighting, food, handling, etc). To create
619 tumors of mixed cell populations, an admixture of 1×10^6 U251-GFP cells and 2×10^6 U87-RFP
620 cells were injected subcutaneously in both flanks. Tumors were allowed to establish for 11

621 days and then 1×10^6 CAR-T cells were administered by tail vein injection. If one or both
622 tumors failed to establish, that animal was excluded from the experiment (n = 1). Mice were
623 monitored daily until tumors became palpable, after which time tumor growth was measured
624 using an electronic caliper every 2-3 days. The volume of the tumor was calculated as length ×
625 $width^2 \times 1/2$. Mice were humanely killed when at least one tumor volume reached $1000mm^3$.
626 Tumors were harvested at the experimental end point and prepared for frozen sections.
627 Tumor samples fixed in 10% buffered formalin overnight were cryoprotected with 10%
628 sucrose to 30% sucrose in PBS sequentially before embedding in OCT (Sakura Finetek, Tokyo,
629 Japan) and freezing on dry ice, with subsequent storage at -80°C. This protocol was selected
630 and optimized to allow maximum retention of soluble fluorescent proteins (GFP/RFP) during
631 tissue processing. Cryosections (5µM) were cut using a Leica CM1950 cryostat and mounted
632 using ProLong Gold with DAPI (Thermo Fisher). Slides were imaged using the Olympus IX73
633 microscope. To minimize bias, fields of view were first selected based on DAPI nuclear staining,
634 before imaging the corresponding GFP and RFP channels. Areas of green and red fluorescence
635 were automatically calculated using ImageJ (NIH). Threshold 21-255 was used for RFP area
636 calculation while threshold 35-255 was used for GFP area calculation. Fluorescence overlays
637 were created by overlaying black and white images and applying false colors using ImageJ.

638

639 **Statistical analysis**

640 Statistical analyses were performed using GraphPad Prism version 5 and OriginPro 8
641 (OriginLab). In addition, the TumGrowth web program
642 (https://kroemerlab.shinyapps.io/TumGrowth/) was used for comparison of tumor growth

643 curves by Type II ANOVA. For Kaplan-Meier Survival analysis, Log Rank method was used to
644 test the Equality over Groups.

645

646 **Acknowledgments**

647 We thank Professors Klaus Pfizenmaier (Institute of Cell Biology and Immunology, University
648 of Stuttgart, Stuttgart, Germany), and Stephen Gottschalk (Department of Bone Marrow
649 Transplantation and Cellular Therapy, St Jude Children's Research Hospital, Memphis, TN,
650 USA), for provision of the FAP-specific MO36 scFv. We are grateful to Professor Bryan Day
651 (QIMR Berghofer Medical Research Institute, Brisbane, Queensland, Australia) for the IIIA4
652 single chain variable fragment used for construction of the EphA3-specific CAR. We also thank
653 Dr Susanne Heinzel, Walter and Eliza Hall Institute of Medical Research, Melbourne Victoria,
654 Australia, for her review and valuable comments on the manuscript.

655

656 **DECLARATIONS**

657 **Ethics approval and consent to participate**

658 Blood collection from healthy donors for CAR-T cell manufacture was approved by the Central
659 Adelaide Local Health Network (CALHN) Human Research Ethics Committee (approval number
660 HREC/16/RAH/191). Blood collection from healthy donors for ECFC generation was approved
661 by the human ethics committees of SA Pathology and the University of South Australia
662 (approval numbers, ethics #85–13 and UniSA HREC #201187 respectively). Written consent to
663 participate was obtained from donors of fresh whole blood, whereas buffy coats obtained
664 from Australian Red Cross Lifeblood were obtained under an approved waiver of consent.

Animal experiments were approved by the University of South Australia Animal Ethics Committee (approval number: 45/17).

Consent for publication

All authors consent to the publication of this manuscript.

Availability of data and materials

Original datasets will be made available upon reasonable request to the corresponding author.

Competing interests

The authors declare that the research was conducted in the absence of any commercial or financial relationships that could be construed as a potential conflict of interest.

Funding

This work was supported by a Beat Cancer Project Hospital Support Package, the Neurosurgical Research Foundation, Tour de Cure, the Ray & Shirl Norman Cancer Research Trust, the Mark Hughes Foundation, and the Health Services Charitable Gifts Board Adelaide. SMP is supported by an NHMRC Senior Research Fellowship #1156693).

Authors' contributions

WY: investigation, methodology, conceptualization, data curation, formal analysis, resources, writing – original draft, writing – review & editing. **NTHT:** Investigation, methodology, formal

688 analysis. **RP:** Investigation, formal analysis. **TG:** Investigation, formal analysis, supervision,
689 writing – review & editing. **MNT:** Resources. **SMP:** Funding acquisition, resources. **MPC:**
690 Resources. **CSB:** Resources. **LME:** Conceptualization, investigation, methodology, data
691 curation, formal analysis, funding acquisition, resources, supervision, writing – original draft,
692 writing – review & editing. **MPB:** Conceptualization, funding acquisition, resources,
693 supervision, writing – review & editing.
694

695 **REFERENCES**

696 1. Stupp R, Mason WP, van den Bent MJ, Weller M, Fisher B, Taphoorn MJ, et al. Radiotherapy plus
697 concomitant and adjuvant temozolomide for glioblastoma. *N Engl J Med*. 2005; **352**: 987-996.
698 2. Field KM, Simes J, Nowak AK, Cher L, Wheeler H, Hovey EJ, et al. Randomized phase 2 study of
699 carboplatin and bevacizumab in recurrent glioblastoma. *Neuro Oncol*. 2015; **17**: 1504-1513.
700 3. Wagner J, Wickman E, DeRenzo C, Gottschalk S. CAR T Cell Therapy for Solid Tumors: Bright
701 Future or Dark Reality? *Mol Ther*. 2020; **28**: 2320-2339.
702 4. Brown MP, Ebert LM, Gargett T. Clinical chimeric antigen receptor-T cell therapy: a new and
703 promising treatment modality for glioblastoma. *Clin Transl Immunology*. 2019; **8**: e1050.
704 5. Ahmed N, Salsman VS, Kew Y, Shaffer D, Powell S, Zhang YJ, et al. HER2-specific T cells target
705 primary glioblastoma stem cells and induce regression of autologous experimental tumors. *Clin*
706 *Cancer Res*. 2010; **16**: 474-485.
707 6. Brown CE, Badie B, Barish ME, Weng L, Ostberg JR, Chang WC, et al. Bioactivity and Safety of
708 IL13Rα2-Redirected Chimeric Antigen Receptor $CD8^+$ T Cells in Patients with Recurrent
709 Glioblastoma. *Clin Cancer Res*. 2015; **21**: 4062-4072.
710 7. Brown CE, Alizadeh D, Starr R, Weng L, Wagner JR, Naranjo A, et al. Regression of Glioblastoma
711 after Chimeric Antigen Receptor T-Cell Therapy. *N Engl J Med*. 2016; **375**: 2561-2569.
712 8. O'Rourke DM, Nasrallah MP, Desai A, Melenhorst JJ, Mansfield K, Morrissette JJD, et al. A single
713 dose of peripherally infused EGFRvIII-directed CAR T cells mediates antigen loss and induces
714 adaptive resistance in patients with recurrent glioblastoma. *Sci Transl Med*. 2017; **9**.
715 9. Brown CE, Aguilar B, Starr R, Yang X, Chang WC, Weng L, et al. Optimization of IL13Rα2-Targeted
716 Chimeric Antigen Receptor T Cells for Improved Anti-tumor Efficacy against Glioblastoma. *Mol*
717 *Ther*. 2018; **26**: 31-44.
718 10. Goff SL, Morgan RA, Yang JC, Sherry RM, Robbins PF, Restifo NP, et al. Pilot Trial of Adoptive
719 Transfer of Chimeric Antigen Receptor-transduced T Cells Targeting EGFRvIII in Patients With
720 Glioblastoma. *J Immunother*. 2019; **42**: 126-135.
721 11. Brown CE, Hibbard JC, Alizadeh D, Blanchard MS, Natri HM, Wang D, et al. Locoregional delivery of
722 IL-13α2-targeting CAR-T cells in recurrent high-grade glioma: a phase 1 trial. *Nat Med*. 2024; **30**:
723 1001-1012.
724 12. Choi BD, Gerstner ER, Frigault MJ, Leick MB, Mount CW, Balaj L, et al. Intraventricular CARv3-
725 TEAM-E T Cells in Recurrent Glioblastoma. *N Engl J Med*. 2024; **390**: 1290-1298.
726 13. Rettig WJ, Garin-Chesa P, Beresford HR, Oettgen HF, Melamed MR, Old LJ. Cell-surface
727 glycoproteins of human sarcomas: differential expression in normal and malignant tissues and
728 cultured cells. *Proc Natl Acad Sci U S A*. 1988; **85**: 3110-3114.
729 14. Ostermann E, Garin-Chesa P, Heider KH, Kalat M, Lamche H, Puri C, et al. Effective
730 immunoconjugate therapy in cancer models targeting a serine protease of tumor fibroblasts. *Clin*
731 *Cancer Res*. 2008; **14**: 4584-4592.
732 15. Kakarla S, Chow KK, Mata M, Shaffer DR, Song XT, Wu MF, et al. Antitumor effects of chimeric
733 receptor engineered human T cells directed to tumor stroma. *Mol Ther*. 2013; **21**: 1611-1620.
734 16. Wang LC, Lo A, Scholler J, Sun J, Majumdar RS, Kapoor V, et al. Targeting fibroblast activation
735 protein in tumor stroma with chimeric antigen receptor T cells can inhibit tumor growth and
736 augment host immunity without severe toxicity. *Cancer Immunol Res*. 2014; **2**: 154-166.
737 17. Lo A, Wang LS, Scholler J, Monslow J, Avery D, Newick K, et al. Tumor-Promoting Desmoplasia Is
738 Disrupted by Depleting FAP-Expressing Stromal Cells. *Cancer Res*. 2015; **75**: 2800-2810.
739 18. Caligiuri G, Tuveson DA. Activated fibroblasts in cancer: Perspectives and challenges. *Cancer Cell*.
740 2023; **41**: 434-449.

741 19. Petrausch U, Schuberth PC, Hagedorn C, Soltermann A, Tomaszek S, Stahel R, et al. Re-directed T
742 cells for the treatment of fibroblast activation protein (FAP)-positive malignant pleural
743 mesothelioma (FAPME-1). *BMC Cancer*. 2012; **12**: 615.
744 20. Schuberth PC, Hagedorn C, Jensen SM, Gulati P, van den Broek M, Mischo A, et al. Treatment of
745 malignant pleural mesothelioma by fibroblast activation protein-specific re-directed T cells. *J*
746 *Transl Med*. 2013; **11**: 187.
747 21. Ebert LM, Yu W, Gargett T, Toubia J, Kollis PM, Tea MN, et al. Endothelial, pericyte and tumor cell
748 expression in glioblastoma identifies fibroblast activation protein (FAP) as an excellent target for
749 immunotherapy. *Clin Transl Immunology*. 2020; **9**: e1191.
750 22. Li M, Li G, Kiyokawa J, Tirmizi Z, Richardson LG, Ning J, et al. Characterization and oncolytic virus
751 targeting of FAP-expressing tumor-associated pericytes in glioblastoma. *Acta Neuropathol*
752 *Commun*. 2020; **8**: 221.
753 23. Tran E, Chinnasamy D, Yu Z, Morgan RA, Lee CC, Restifo NP, et al. Immune targeting of fibroblast
754 activation protein triggers recognition of multipotent bone marrow stromal cells and cachexia. *J*
755 *Exp Med*. 2013; **210**: 1125-1135.
756 24. Gulati P, Ruhl J, Kannan A, Pircher M, Schuberth P, Nytko KJ, et al. Aberrant Lck Signal via CD28
757 Costimulation Augments Antigen-Specific Functionality and Tumor Control by Redirected T Cells
758 with PD-1 Blockade in Humanized Mice. *Clin Cancer Res*. 2018; **24**: 3981-3993.
759 25. A. Curioni CB, S. Hiltbrunner, L. Bankel, P. Gulati, W. Weder, I. Opitz,O. Lauk, C. Caviezel, A. Knuth,
760 C.Mu¨nz, C. Renner, R.A. Stahel, U. Petrausch. A phase I clinical trial of malignant pleural
761 mesothelioma treated with locally delivered autologous anti-FAP-targeted CAR T-cells. *Annals of*
762 *Oncology*. 2019; **30** (Supplement 5): v501
763 26. Brocks B, Garin-Chesa P, Behrle E, Park JE, Rettig WJ, Pfizenmaier K, et al. Species-crossreactive
764 scFv against the tumor stroma marker "fibroblast activation protein" selected by phage display
765 from an immunized FAP-/- knock-out mouse. *Mol Med*. 2001; **7**: 461-469.
766 27. Upadhyay R, Boiarsky JA, Pantsulaia G, Svensson-Arvelund J, Lin MJ, Wroblewska A, et al. A Critical
767 Role for Fas-Mediated Off-Target Tumor Killing in T-cell Immunotherapy. *Cancer Discov*. 2021; **11**:
768 599-613.
769 28. Bonnotte B, Favre N, Reveneau S, Micheau O, Droin N, Garrido C, et al. Cancer cell sensitization to
770 fas-mediated apoptosis by sodium butyrate. *Cell Death Differ*. 1998; **5**: 480-487.
771 29. Monjazeb AM, Hsiao HH, Sckisel GD, Murphy WJ. The role of antigen-specific and non-specific
772 immunotherapy in the treatment of cancer. *J Immunotoxicol.* 2012; **9**: 248-258.
773 30. Ma HL, Whitters MJ, Konz RF, Senices M, Young DA, Grusby MJ, et al. IL-21 activates both innate
774 and adaptive immunity to generate potent antitumor responses that require perforin but are
775 independent of IFN-gamma. *J Immunol.* 2003; **171**: 608-615.
776 31. Smyth MJ, Swann J, Kelly JM, Cretney E, Yokoyama WM, Diefenbach A, et al. NKG2D recognition
777 and perforin effector function mediate effective cytokine immunotherapy of cancer. *J Exp Med*.
778 2004; **200**: 1325-1335.
779 32. Liu RB, Engels B, Schreiber K, Ciszewski C, Schietinger A, Schreiber H, et al. IL-15 in tumor
780 microenvironment causes rejection of large established tumors by T cells in a noncognate T cell
781 receptor-dependent manner. *Proc Natl Acad Sci U S A*. 2013; **110**: 8158-8163.
782 33. Glynn JJ, Hinds MT. Endothelial outgrowth cells: function and performance in vascular grafts.
783 *Tissue Eng Part B Rev*. 2014; **20**: 294-303.
784 34. Busek P, Balaziova E, Matrasova I, Hilser M, Tomas R, Syrucek M, et al. Fibroblast activation
785 protein alpha is expressed by transformed and stromal cells and is associated with mesenchymal
786 features in glioblastoma. *Tumour Biol*. 2016; **37**: 13961-13971.
787 35. Perrin SL, Samuel MS, Koszyca B, Brown MP, Ebert LM, Oksdath M, et al. Glioblastoma
788 heterogeneity and the tumour microenvironment: implications for preclinical research and
789 development of new treatments. *Biochem Soc Trans*. 2019; **47**: 625-638.

790 36. Galli R, Binda E, Orfanelli U, Cipelletti B, Gritti A, De Vitis S, et al. Isolation and characterization of
791 tumorigenic, stem-like neural precursors from human glioblastoma. *Cancer Res*. 2004; **64**: 7011-
792 7021.
793 37. Pollard SM, Yoshikawa K, Clarke ID, Danovi D, Stricker S, Russell R, et al. Glioma stem cell lines
794 expanded in adherent culture have tumor-specific phenotypes and are suitable for chemical and
795 genetic screens. *Cell Stem Cell*. 2009; **4**: 568-580.
796 38. Stringer BW, Day BW, D'Souza RCJ, Jamieson PR, Ensbey KS, Bruce ZC, et al. A reference collection
797 of patient-derived cell line and xenograft models of proneural, classical and mesenchymal
798 glioblastoma. *Sci Rep*. 2019; **9**: 4902.
799 39. Vanderlugt CJ, Miller SD. Epitope spreading. *Curr Opin Immunol*. 1996; **8**: 831-836.
800 40. Fleischer B. Lysis of bystander target cells after triggering of human cytotoxic T lymphocytes. *Eur J*
801 *Immunol.* 1986; **16**: 1021-1024.
802 41. Lanzavecchia A. Is the T-cell receptor involved in T-cell killing? *Nature*. 1986; **319**: 778-780.
803 42. Hong LK, Chen Y, Smith CC, Montgomery SA, Vincent BG, Dotti G, et al. CD30-Redirected Chimeric
804 Antigen Receptor T Cells Target $CD30^+$ and $CD30^-$ Embryonal Carcinoma via Antigen-Dependent
805 and Fas/FasL Interactions. *Cancer Immunol Res*. 2018; **6**: 1274-1287.
806 43. Benmebarek MR, Karches CH, Cadilha BL, Lesch S, Endres S, Kobold S. Killing Mechanisms of
807 Chimeric Antigen Receptor (CAR) T Cells. *Int J Mol Sci*. 2019; **20:** 1283
808 44. Zaidi MR. The Interferon-Gamma Paradox in Cancer. *J Interferon Cytokine Res*. 2019; **39**: 30-38.
809 45. Idriss HT, Naismith JH. TNF alpha and the TNF receptor superfamily: structure-function
810 relationship(s). *Microsc Res Tech*. 2000; **50**: 184-195.
811 46. Michie J, Beavis PA, Freeman AJ, Vervoort SJ, Ramsbottom KM, Narasimhan V, et al. Antagonism
812 of IAPs Enhances CAR T-cell Efficacy. *Cancer Immunol Res*. 2019; **7**: 183-192.
813 47. Song EZ, Wang X, Philipson BI, Zhang Q, Thokala R, Zhang L, et al. The IAP antagonist birinapant
814 enhances chimeric antigen receptor T cell therapy for glioblastoma by overcoming antigen
815 heterogeneity. *Mol Ther Oncolytics*. 2022; **27**: 288-304.
816 48. Tough DF, Borrow P, Sprent J. Induction of bystander T cell proliferation by viruses and type I
817 interferon in vivo. *Science*. 1996; **272**: 1947-1950.
818 49. Murali-Krishna K, Altman JD, Suresh M, Sourdive D, Zajac A, Ahmed R. In vivo dynamics of anti-
819 viral CD8 T cell responses to different epitopes. An evaluation of bystander activation in primary
820 and secondary responses to viral infection. *Adv Exp Med Biol*. 1998; **452**: 123-142.
821 50. Kim TS, Shin EC. The activation of bystander $CD8^+$ T cells and their roles in viral infection. *Exp Mol*
822 *Med.* 2019; **51**: 1-9.
823 51. Rosenberg SA. IL-2: the first effective immunotherapy for human cancer. *J Immunol*. 2014; **192**:
824 5451-5458.
825 52. Rollings CM, Sinclair LV, Brady HJM, Cantrell DA, Ross SH. Interleukin-2 shapes the cytotoxic T cell
826 proteome and immune environment-sensing programs. *Sci Signal*. 2018; **11**: eaap8112
827 53. Maykel J, Liu JH, Li H, Shultz LD, Greiner DL, Houghton J. NOD-scidIl2rg (tm1Wjl) and NOD-Rag1
828 (null) Il2rg (tm1Wjl) : a model for stromal cell-tumor cell interaction for human colon cancer. *Dig*
829 *Dis Sci*. 2014; **59**: 1169-1179.
830 54. Oyler-Yaniv A, Oyler-Yaniv J, Whitlock BM, Liu Z, Germain RN, Huse M, et al. A Tunable Diffusion-
831 Consumption Mechanism of Cytokine Propagation Enables Plasticity in Cell-to-Cell
832 Communication in the Immune System. *Immunity*. 2017; **46**: 609-620.
833 55. Rahman M, Reyner K, Deleyrolle L, Millette S, Azari H, Day BW, et al. Neurosphere and adherent
834 culture conditions are equivalent for malignant glioma stem cell lines. *Anat Cell Biol*. 2015; **48**: 25-
835 35.
836 56. Schroeder HW, Jr., Cavacini L. Structure and function of immunoglobulins. *J Allergy Clin Immunol*.
837 2010; **125**: S41-52.
838 57. Nirula A, Glaser SM, Kalled SL, Taylor FR. What is IgG4? A review of the biology of a unique
839 immunoglobulin subtype. *Curr Opin Rheumatol*. 2011; **23**: 119-124.

840 58. Hudecek M, Sommermeyer D, Kosasih PL, Silva-Benedict A, Liu L, Rader C, et al. The nonsignaling
841 extracellular spacer domain of chimeric antigen receptors is decisive for in vivo antitumor activity.
842 *Cancer Immunol Res*. 2015; **3**: 125-135.
843 59. Jonnalagadda M, Mardiros A, Urak R, Wang X, Hoffman LJ, Bernanke A, et al. Chimeric antigen
844 receptors with mutated IgG4 Fc spacer avoid fc receptor binding and improve T cell persistence
845 and antitumor efficacy. *Mol Ther*. 2015; **23**: 757-768.
846 60. Martin-Ramirez J, Hofman M, van den Biggelaar M, Hebbel RP, Voorberg J. Establishment of
847 outgrowth endothelial cells from peripheral blood. *Nat Protoc*. 2012; **7**: 1709-1715.
848 61. Fouladzadeh A, Dorraki M, Min KKM, Cockshell MP, Thompson EJ, Verjans JW, et al. The
849 development of tumour vascular networks. *Commun Biol*. 2021; **4**: 1111.

850

851

852 **FIGURE LEGENDS**

853 **Figure 1. Structure and characterization of the FAP-CAR. (a)** Schematic representation of the
854 FAP CAR construct. The CAR consisted of the MO36 anti-FAP scFv linked to a CD28
855 transmembrane (TM) and CD28 and CD3ζ costimulatory endodomains. The FAP-CAR contains
856 the myc tag at the end of the scFv and a spacer from human IgG4 CH2CH3 fragment with
857 several point mutations. **(b)** CAR expression on CAR-T cells was detected by flow cytometry.
858 The CAR-T cells were stained by FITC-conjugated anti-myc tag antibody. One representative
859 sample from 8 donors is shown. **(c)** FAP expression on target cell lines was confirmed by flow
860 cytometry. **(d)** CAR-transduced or non-transduced T cells were co-cultured with target cells
861 with or without FAP expression and the IL-2 concentration in supernatants determined 48h
862 later. The data represent the mean ± SE from three independent assays. Each assay
863 represents the average value from duplicate wells. Anti-EphA3 CAR-T cells provided the
864 irrelevant CAR in this assay. (e-f): FAP-CAR-T cell products were manufactured from 5 different
865 healthy donors and analysed by flow cytometry, using an antibody to the myc tag to identify
866 the CAR^+ (transduced) cells. Shown in **(e)** is a summary of the CD4:CD8 ratio within the CAR^+
867 and CAR^- populations, while **(f)** depicts the memory phenotype; pie charts show mean values
868 across the 5 donors. T cells were categorized as TSCM/Naïve ($CCR7^+/CD45RA^+$), TCM
869 ($CCR7^+/CD45RA^-$), TEM ($CCR7^-/CD45RA^-$), and TEMRA ($CCR7^-/CD45RA^+$).

870

871 **Figure 2. FAP-CAR-T cells display cytotoxic activity against glioblastoma cell lines and GNS**
872 **cells expressing varying levels of FAP.** Left panels: FAP expression on target cells was
873 examined by flow cytometry. Red dotted lines indicate isotype control and black solid lines

874 indicate anti-FAP antibody. Centre and right panels: Target cells were established in a
875 CytoView-Z plate and placed in the Maestro Z system for up to 24h, followed by addition of
876 FAP-CAR-T cells as effectors or non-transduced T cells (NT-T) as a control. Cytotoxicity was
877 monitored over time and represented as percentage of target lysis averaged across duplicate
878 wells. Representative examples shown in centre panels and % cytolysis at 48h after effector
879 cell addition is plotted in the right panels. The effector:target (E:T) ratio is indicated. *t*-test; * P
880 < 0.05, ** $P < 0.01$. (a) FAP^+ U87 and FAP^- U251 cells were used as target cells. The data
881 represents the mean ± SE from three independent assays. Each assay represents the average
882 value from duplicate wells. (b) GNS cells expressing varying levels of FAP were used as target
883 cells. The data represent the mean ± SE from 3-5 independent assays. Each assay represents
884 the average value from duplicate wells.

885

886 **Figure 3: FAP-CAR-T cells exert a bystander killing effect on FAP^- tumor cells after CAR**
887 **engagement.** FAP^+ tumor cells were stained with cell trace far red (CTFR) for discrimination
888 and then FAP^+ and FAP^- tumor cells were mixed at a 1:1 ratio, followed by treatment with
889 either FAP-CAR-T cells or non-transduced T cells (NT-T) at a 1:1 E:T ratio. Single cultured target
890 cells were treated in the same way as control. The viability of target cells was analyzed 48h
891 later by flow cytometry using fixable viability dye (FVD). **(a)** FAP expression on target cells was
892 examined by flow cytometry. The FAP^- SJH-1 and RKI-1 GNS cell lines are shown here; refer to
893 Fig 2 for FAP^+ MN1 and CCB-G3-C cells. Red dotted lines indicate isotype control and black
894 solid lines indicate anti-FAP antibody. **(b)** Gating strategy of a representative experiment (Pair
895 1) showing cell death within the FAP^- target cell population. Refer to Supplementary Figure 3

896 for representative examples of cell death within the FAP^+ target cell population. **(c-d)** The
897 percentage of cell death of FAP^- GNS cells (**c**) or FAP^+ GNS cells (**d**) after 48h co-culture was
898 calculated. Data were pooled from three independent experiments, including both Pair 1 and
899 Pair 2 samples (total n = 5-6). Samples from both Pair one and Pair two were pooled together.
900 *t*-test; * $P < 0.05$, *** $P < 0.001$.

901 **Figure 4: Bystander killing by FAP-CAR-T cells can be mediated by soluble factors. (a)**
902 Schematic of assay set-up. **(b)** Representative fluorescence images of Hoechst 33258 (left) and
903 PI (right) staining on FAP^- tumor cells cultured in upper chambers for 48h. Effector cells (NT-T
904 cells or FAP-CAR-T cells) added to lower chambers are indicated. Images were collected using
905 a 10X objective. **(c-d)** Quantification of percent of FAP^- target cell death in upper chamber.
906 Shown in c is FAP^- RKI-1 from Pair 1, n = 6, pooled from 3 experiments. Shown in **d** is FAP^- SJH-
907 1 from Pair 2, n = 4 pooled from 2 experiments. Each dot represents the mean percentage of
908 cell death from 3 fields of view of each well. *t*-test; * $P < 0.05$, ** $P < 0.01$. **(e)** Concentrations
909 of secreted factors in supernatants of cocultures were determined by Legendplex kit. FAP-
910 CAR-T stimulated by the FAP^+ GNS cell line CCB-G6-T was used as positive control.
911 Supernatants were collected after 48h. Data are pooled from 3 experiments except NT-T of
912 Pair 2 which only have two data points. Mann-Whitney *U*-tests; * $P < 0.05$.

913

914 **Figure 5. IL-2 induces T cells to exert antigen nonspecific cytotoxicity against GNS cells. (a)** A
915 conceptual diagram of the theory. After antigen-specific activation, FAP-CAR-T cells secrete IL-
916 2 which mobilizes NT-T cells to exert further cytotoxicity against tumor cells. **(b)** Cytotoxicity
917 assay of FAP-CAR-T or NT-T cells against MN1 GNS cells, with or without exogenous IL-2

918 (20ng/ml). FAP$^+$ MN1 cells were established in a CytoView-Z plate for 24h before addition of
919 effector cells. Target cell growth was monitored by impedance values in real time by the
920 Maestro Z system. Time-course graphs for varying E:T ratios, as indicated, show target lysis as %
921 cytotoxicity. A summary of % cytolysis at 36h after effector cell addition is shown bottom right.
922 Data points represent mean ± SEM from 3 independent experiments. Each assay represents
923 the average value from duplicate wells. **(c)** Secreted factors were measured in supernatants
924 50h after addition of effector cells using Legendplex assay. A total of 12 analytes were
925 measured in 3 experiments (or 2 experiments for MN-1 and MN-1/IL-2 controls). Results of 6
926 key cytotoxic factors are shown, with the other 6 being depicted in Supplementary Figure 6.
927 Statistical analysis of these data is presented in Table 1.

928

929 **Figure 6. FAP-CAR-T cells control tumor growth in a mouse model with heterogeneous**
930 **antigen expression. (a)** *In vitro* bystander killing assay of FAP$^-$ U251-GFP and FAP$^+$ U87-RFP.
931 Cells were cultured individually or together and were treated with FAP-CAR-T or NT-T cells.
932 Fluorescence images were taken 24h later and GFP and RFP positive cells were counted using
933 ImageJ. Graphs show mean and SE from 6 counts (3 fields of views × 2 repeats). Effector cells
934 derived from one donor were used **(b)** ECFCs were co-cultured with an equal number of U87-
935 RFP and U251-GFP cells and subsequently treated with effector cells (either FAP-CAR-T or NT-
936 T cells) or left untreated (indicated as -). After 48 hours, cell counts were determined using
937 flow cytometry and fold change from baseline calculated. The assay was performed three
938 times, with FAP-CAR-T or NT-T cells derived from three different donors. Graphs show mean
939 and SEM. **(c-f)** Subcutaneous tumours were created on both flanks of NSG mice using a

940 mixture of FAP^- U251-eGFP and FAP^+ U87-RFP cells (as illustrated in the inset to **d**). Tumors
941 were allowed to establish for 21 days and then mice were treated with a single intravenous
942 injection of 1 x 10^6 FAP-CAR-T cells (blue) or NT-T cells (grey) or left untreated (black). FAP-
943 CAR-T group n = 11, NT-T group n = 9, untreated group n = 14. (**c**) Representative tumor tissue
944 section showing the balance of U251 (green) and U87 (red) cells, with DAPI staining to
945 visualize nuclei. **(d)** Tumor growth curves for each mouse. The volume of tumors on each flank
946 was measured every 2-3 days and summated to calculate total tumor load per mouse. Tumor
947 growth in FAP-CAR-T group was significantly lower than untreated or NT-T groups (both
948 adjusted $P < 0.0001$; Type II ANOVA using TumGrowth analysis). **(e)** Animals were humanely
949 killed once at least one tumor reached 1000 mm^3 and survival analysis performed using a
950 Kaplan–Meier plot. $P < 0.0001$ by Log-Rank test. **(f)** GFP and RFP area of endpoint tumor
951 sections were calculated. Data are pooled from a total of 28 sections from 13 tumors of FAP-
952 CAR-T treated group, 27 sections from 13 tumors of NT-T treated group and 20 sections from
953 9 tumors of untreated group. "□" represents mean; "x" represents minimal and maximal data;
954 Bar represent 1% and 99% data distribution; Box represents 25%, 50% and 75% data
955 distribution. *t*-test; * $P < 0.05$, ** $P < 0.01$, *** $P < 0.001$

956

957

Figure 1

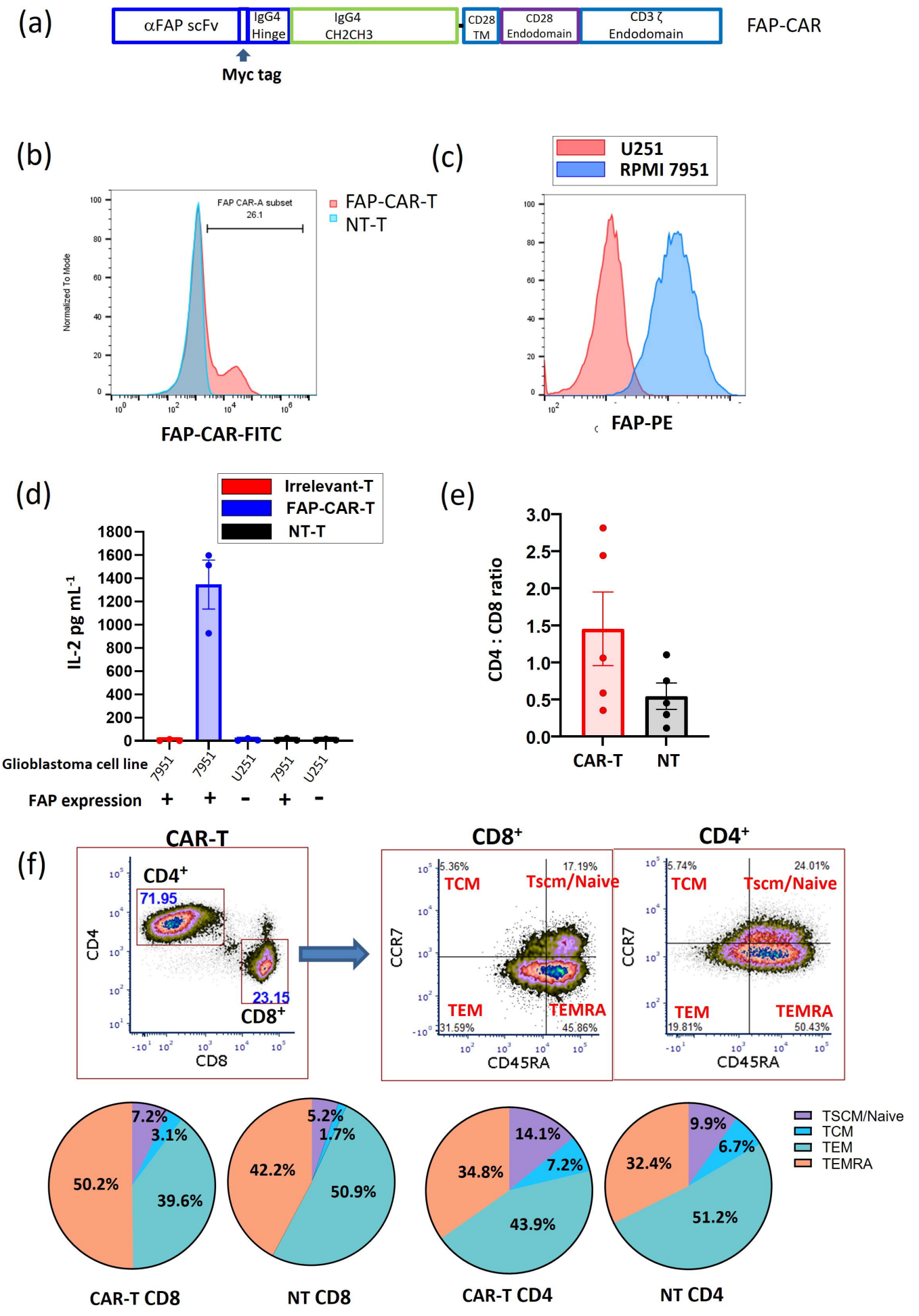
(a)
αFAP scFv
IgG4 Hinge
IgG4 CH2CH3
CD28 TM
CD28 Endodomain
CD3 ζ Endodomain
FAP-CAR
Myc tag
(b)
FAP CAR-A subset 26.1
FAP-CAR-T
NT-T
Normalized To Mode
FAP-CAR-FITC
(c)
U251
RPMI 7951
FAP-PE
(d)
Irrelevant-T
FAP-CAR-T
NT-T
IL-2 pg mL-1
Glioblastoma cell line
7951
7951
U251
7951
U251
FAP expression
+
+
-
+
-
(e)
CD4 : CD8 ratio
CAR-T
NT
(f)
CAR-T
CD4+
71.95
23.15
CD8+
CD4
CD8
CD8+
5.36%
17.19%
TCM
Tscm/Naive
TEM
TEMRA
31.59%
45.86%
CCR7
CD45RA
CD4+
5.74%
24.01%
TCM
Tscm/Naive
TEM
TEMRA
19.81%
50.43%
CCR7
CD45RA
7.2%
3.1%
50.2%
39.6%
CAR-T CD8
5.2%
1.7%
42.2%
50.9%
NT CD8
14.1%
7.2%
34.8%
43.9%
CAR-T CD4
9.9%
6.7%
32.4%
51.2%
NT CD4
TSCM/Naive
TCM
TEM
TEMRA

Figure 2

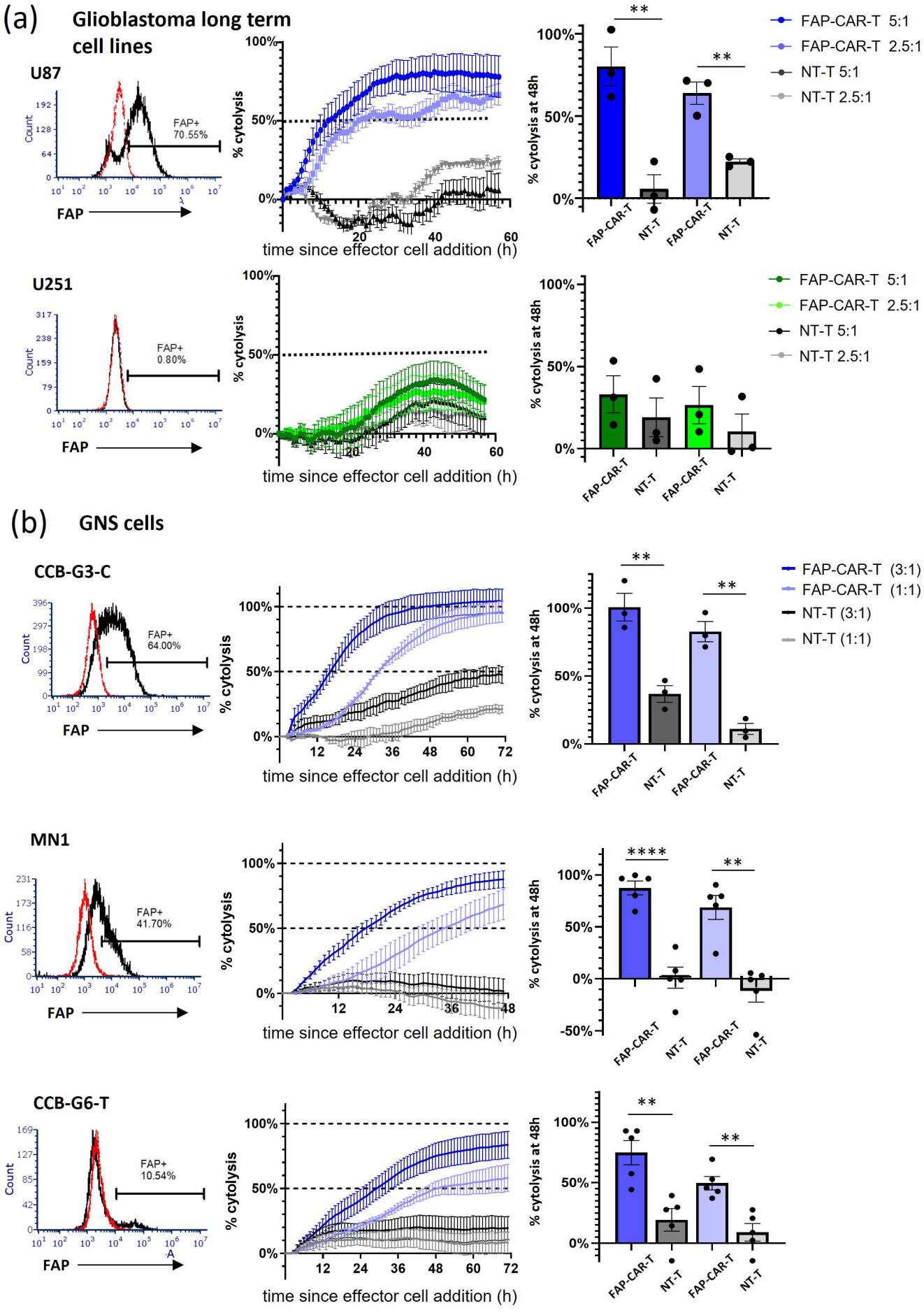
(a)
Glioblastoma long term cell lines
U87
FAP+ 70.55%
Count
FAP
% cytolysis
time since effector cell addition (h)
% cytolysis at 48h
FAP-CAR-T 5:1
FAP-CAR-T 2.5:1
NT-T 5:1
NT-T 2.5:1
FAP-CAR-T
NT-T
U251
FAP+ 0.80%
(b)
GNS cells
CCB-G3-C
FAP+ 64.00%
FAP-CAR-T (3:1)
FAP-CAR-T (1:1)
NT-T (3:1)
NT-T (1:1)
MN1
FAP+ 41.70%
CCB-G6-T
FAP+ 10.54%

Figure 3

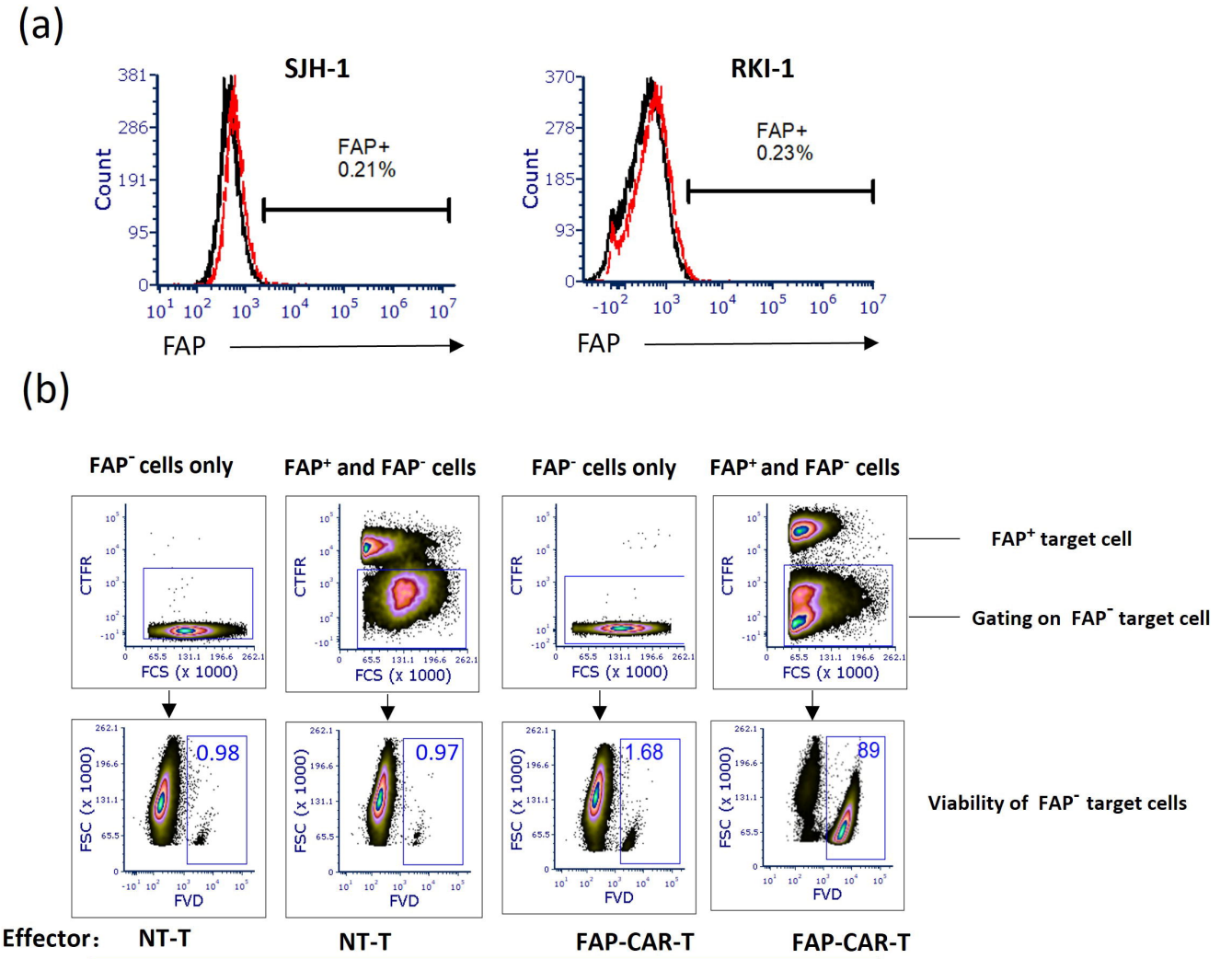
(a)
SJH-1
RKI-1
Count
FAP+
0.21%
FAP+
0.23%
FAP
(b)
FAP⁻ cells only
FAP⁺ and FAP⁻ cells
FAP⁻ cells only
FAP⁺ and FAP⁻ cells
CTFR
FCS (x 1000)
FAP⁺ target cell
Gating on FAP⁻ target cell
FSC (x 1000)
FVD
0.98
0.97
1.68
89
Viability of FAP⁻ target cells
Effector: NT-T
NT-T
FAP-CAR-T
FAP-CAR-T

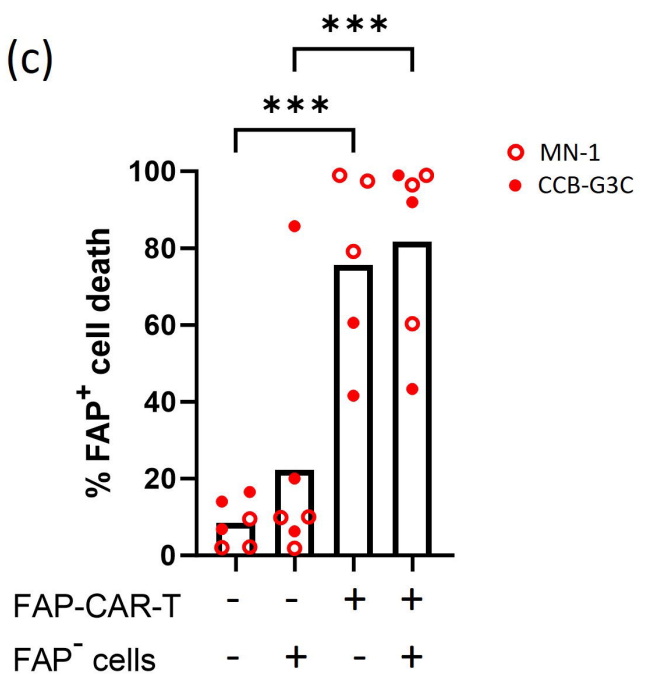
(c)
***
***
MN-1
CCB-G3C
% FAP⁺ cell death
FAP-CAR-T - - + +
FAP⁻ cells - + - +

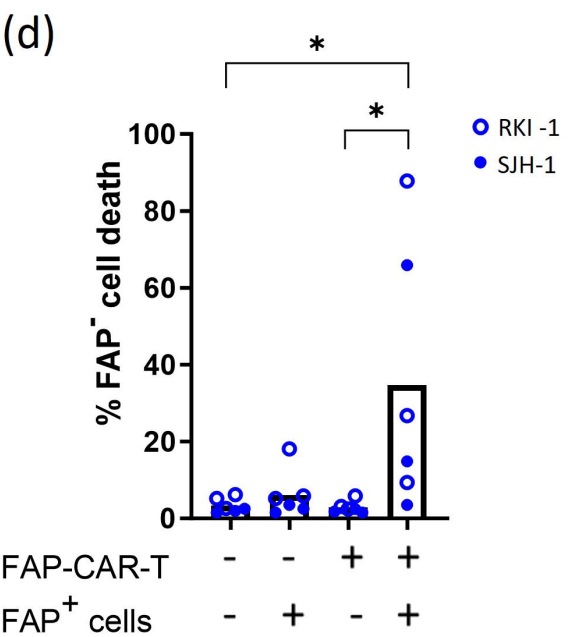
(d)
*
*
RKI -1
SJH-1
% FAP⁻ cell death
FAP-CAR-T - - + +
FAP⁺ cells - + - +

Figure 4

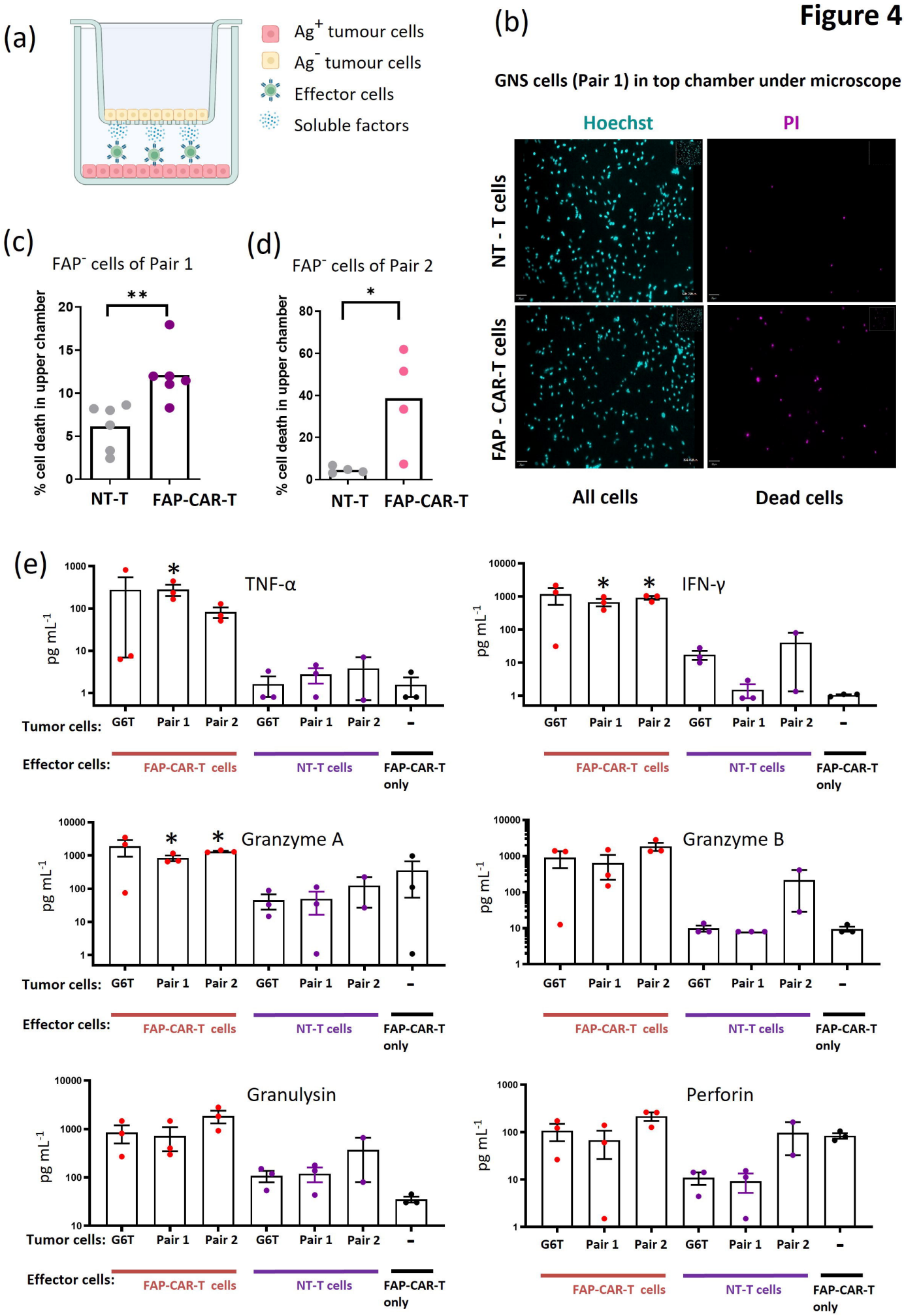
(a)
Ag+ tumour cells
Ag- tumour cells
Effector cells
Soluble factors
(b)
GNS cells (Pair 1) in top chamber under microscope
Hoechst
PI
NT - T cells
FAP - CAR-T cells
All cells
Dead cells
(c)
FAP- cells of Pair 1
% cell death in upper chamber
NT-T
FAP-CAR-T
(d)
FAP- cells of Pair 2
% cell death in upper chamber
NT-T
FAP-CAR-T
(e)
TNF-α
IFN-γ
Granzyme A
Granzyme B
Granulysin
Perforin
pg mL-1
Tumor cells: G6T Pair 1 Pair 2 G6T Pair 1 Pair 2 –
Effector cells: FAP-CAR-T cells NT-T cells FAP-CAR-T only

Figure 5

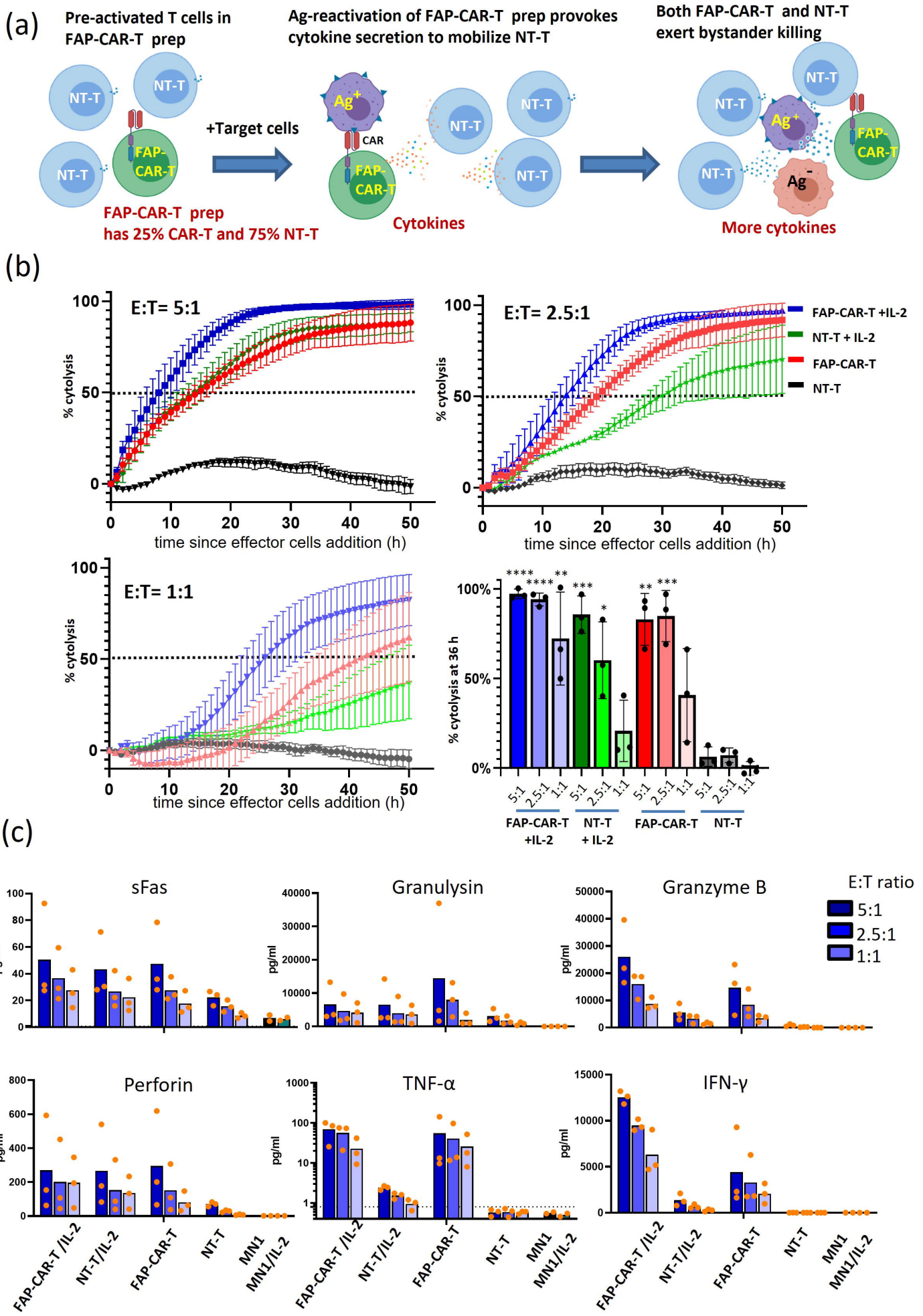
(a)
Pre-activated T cells in FAP-CAR-T prep
Ag-reactivation of FAP-CAR-T prep provokes cytokine secretion to mobilize NT-T
Both FAP-CAR-T and NT-T exert bystander killing
NT-T
FAP-CAR-T
+Target cells
Ag+
CAR
Cytokines
Ag-
More cytokines
FAP-CAR-T prep has 25% CAR-T and 75% NT-T
(b)
E:T= 5:1
E:T= 2.5:1
E:T= 1:1
% cytolysis
time since effector cells addition (h)
FAP-CAR-T +IL-2
NT-T + IL-2
FAP-CAR-T
NT-T
% cytolysis at 36 h
5:1
2.5:1
1:1
(c)
sFas
Granulysin
Granzyme B
Perforin
TNF-α
IFN-γ
pg/ml
E:T ratio
FAP-CAR-T /IL-2
NT-T/IL-2
FAP-CAR-T
NT-T
MN1
MN1/IL-2

Figure 6

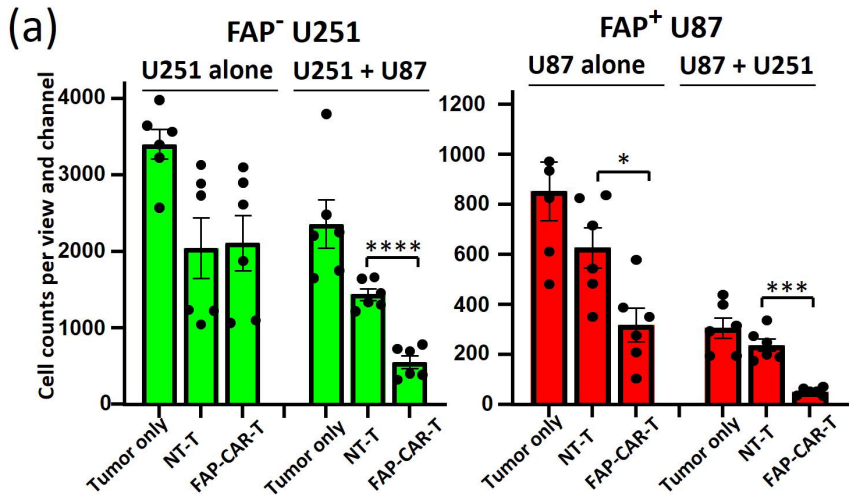
(a)
FAP⁻ U251
U251 alone
U251 + U87
Cell counts per view and channel
4000
3000
2000
1000
0
****
Tumor only
NT-T
FAP-CAR-T
FAP⁺ U87
U87 alone
U87 + U251
1200
1000
800
600
400
200
0
*
***

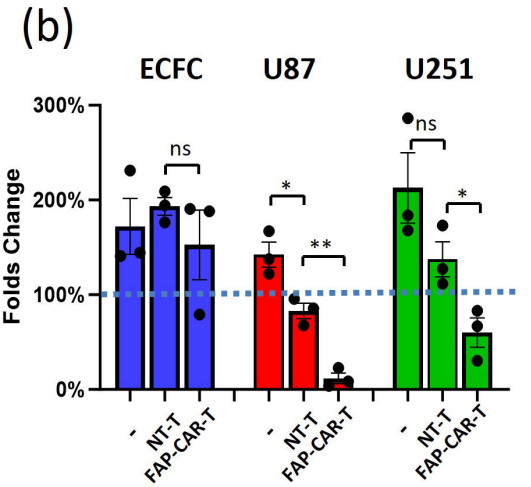
(b)
ECFC
U87
U251
Folds Change
300%
200%
100%
0%
ns
*
**
ns
*
-
NT-T
FAP-CAR-T

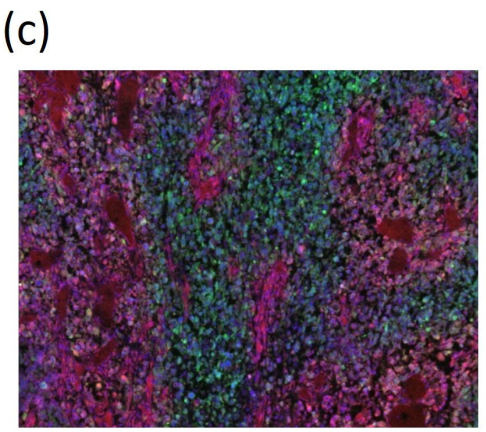
(c)
FAP⁺ RFP⁻ U87 + FAP⁻ eGFP⁺ U251

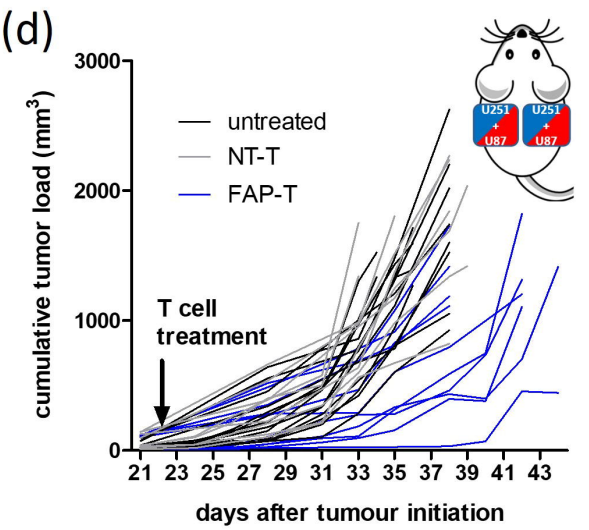
(d)
cumulative tumor load (mm³)
3000
2000
1000
0
untreated
NT-T
FAP-T
T cell
treatment
U251
+
U87
21 23 25 27 29 31 33 35 37 39 41 43
days after tumour initiation

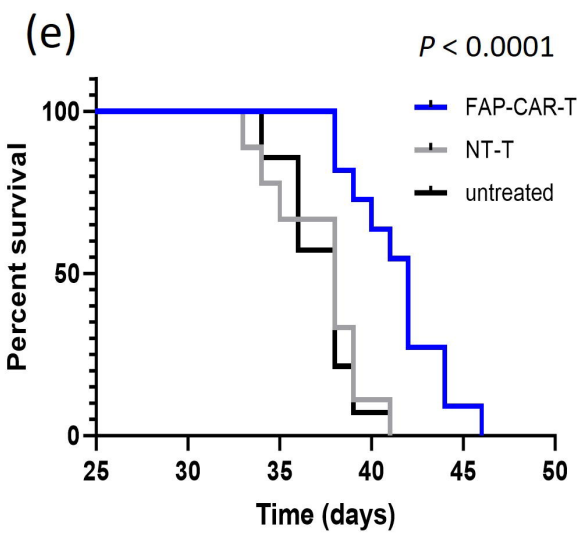
(e)
P < 0.0001
FAP-CAR-T
NT-T
untreated
Percent survival
100
50
0
25 30 35 40 45 50
Time (days)

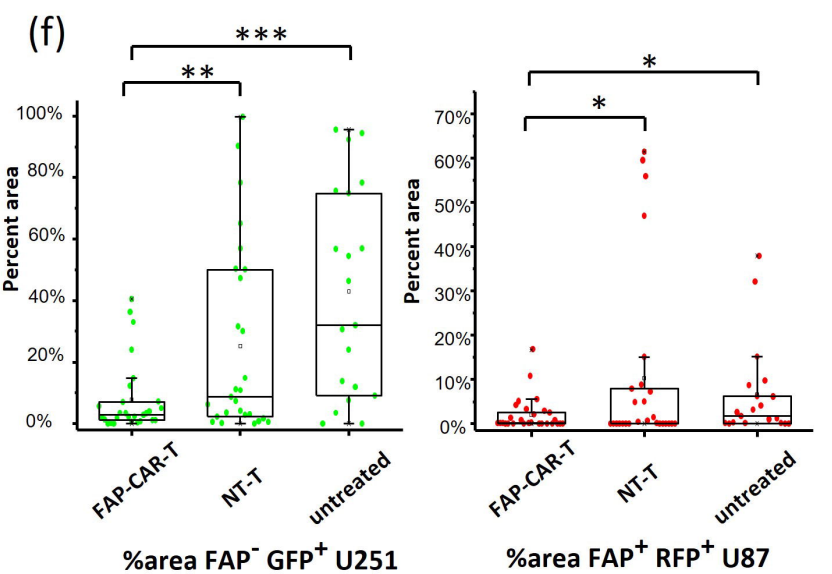
(f)
***
**
Percent area
100%
80%
60%
40%
20%
0%
FAP-CAR-T
NT-T
untreated
%area FAP⁻ GFP⁺ U251
*
*
70%
60%
50%
40%
30%
20%
10%
0%
%area FAP⁺ RFP⁺ U87